IEEE Access
Multidisciplinary ⋮ Rapid Review ⋮ Open Access Journal

Received 31 August 2022, accepted 23 September 2022, date of publication 26 September 2022, date of current version 5 October 2022.

Digital Object Identifier 10.1109/ACCESS.2022.3209996

RESEARCH ARTICLE

Multi-Objective Optimization Framework for Optimal Power Flow Problem of Hybrid Power Systems Considering Security Constraints

SUNDARAM B. PANDYA[1], SOWMYA RAVICHANDRAN[2], PREMKUMAR MANOHARAN[3], (Member, IEEE), PRADEEP JANGIR[4], AND HASSAN HAES ALHELOU[5], (Senior Member, IEEE)

[1]Department of Electrical Engineering, Shri K. J. Polytechnic, Bharuch, Gujarat 392001, India
[2]Department of Electrical and Electronics Engineering, National Institute of Technology, Tiruchirappalli, Tamil Nadu 620015, India
[3]Department of Electrical and Electronics Engineering, Dayananda Sagar College of Engineering, Bengaluru, Karnataka 560078, India
[4]Rajasthan Rajya Vidyut Prasaran Nigam Ltd., Sikar, Rajasthan 332025, India
[5]Department of Electrical Power Engineering, Tishreen University, Lattakia 2230, Syria

Corresponding author: Hassan Haes Alhelou (alhelou@ieee.org) and Premkumar Manoharan (mprem.me@gmail.com)

ABSTRACT The hybrid model of the power system infrastructure is an essential part of the sophisticated technology of the electrical network. Generally, for the Optimal Power Flow (OPF) problem, the power system with only thermal generators is considered. In traditional OPF problems, the fuel cost required to produce electrical energy is considered, and emissions are frequently neglected. Renewable Energy Sources (RESs) have received increasing attention due to various potential characteristics such as clean, diversity, and renewability. As a result, RESs are being integrated into the existing electrical grid at an increasing rate. The study in this paper proposes a techno-economic investigation into the single- and multi-objective OPF, coordinating with RESs, such as wind, PhotoVoltaic (PV), and small hydropower units with hybrid PV. Moreover, the probability density functions of Weibull, Lognormal, and Gumble have been used to predict the required power. A recently reported equilibrium optimizer and its multi-objective version are considered for handling OPF problems. The superior performance of the equilibrium optimizer is further verified with the results of both single- and multi-objective through comparative analysis with state-of-the-art counterparts, and the indications are that the suggested algorithm can find better optimal solutions in a smaller number of generations (iterations) with faster convergence and well distributed optimal Pareto front for multi-objective problems. The results are verified by employing an IEEE-30 bus hybrid power network, and performance comparisons are made among well-established algorithms. Simulation findings show that the suggested algorithm can achieve a reasonable compromise solution for different objectives.

INDEX TERMS Equilibrium optimizer, multiobjective algorithm, optimal power flow, renewable energy sources, security constraints.

I. INTRODUCTION

The Optimal Power Flow (OPF) has become recognized as one of the more challenging problems that must be handled in the planning and operation of modernized power systems. It is anticipated that the power system would need to be run in the best possible condition to provide the highest possible levels of security and reliability. Essentially, the OPF is a multi-model, non-linear minimization problem with high-dimensional features and great computational complexity. Modern society's socioeconomic expansion has posed a great challenge to the electrical power grid. Energy consumption rises each day as the demand for customers grows exponentially. Meanwhile, rising electricity consumption

The associate editor coordinating the review of this manuscript and approving it for publication was Ruisheng Diao.

and the rapid depletion of natural resources could present major supply and demand management problems for utilities [1], [2], [3]. To address this problem, an attractive alternative is to use price-based load management programs to encourage users to alter existing consumption patterns or to deploy on-site distributed Renewable Energy Sources (RESs) to improve power network performance, dependability, reliability, and profitability. Integration of information and communication tools with grid systems pushes the development of conventional grids into smart grids [4], [5], [6]. In this regard, control design system components must be considered and incorporated into the OPF analysis. The OPF is an important strategy for calculating transmission and distribution system power losses as well as power generating costs. The most fundamental and crucial way of managing and controlling an electrical network is the OPF method. The primary purpose of OPF is to define the network's stable operating condition by achieving a certain goal while adhering to equality and inequality constraints [7], [8], [9]. Carpentier [10] was the first to introduce it, and it has been studied over the past half-century. The OPF's traditional objective has been to build coal-based generation systems that run on fossil fuels. Because of the growing usage of sustainable power in the power system, the assessment of the OPF is particularly important after incorporating the irregularity of these renewable units of energy. Researchers from entirely over the world have examined OPF pertaining to thermal-based power generation units [11], [12], [13], [14].

The OPF techniques are regarded as a fundamental and crucial resource for power system operators to assure the sustainability and stability of the system. The OPF algorithms are typically executed at defined time frames to optimize system operation to adjust the values of several dependent parameters to their optimal setting. Numerous researchers have utilized traditional OPF procedures that examine the Economic Environment Dispatch (EED) problem but cater to thermal-based electrical power generators, resulting in CO_2 emissions [15], [16]. The OPF problem is complicated from an economic and computational standpoint. In the context of an economic power network, load flow can be viewed as a problem of Economic Load Dispatch (ELD) to lower the generation costs. The ELD appears to be unable to deal with many operating constraints. The demand non-linearities, losses during the transmission, and the capacity of the generation units can add to the complexity of the load or power flow problem. During its operation, the OPF identifies the optimal values for several control variables, which adds to the computing complexity. The Multi-Objective Grey Wolf Optimizer (MOGWO) can find the Pareto optimal front of any shape. Finally, the result of a complex real-world Multi-Objective OPF (MOOPF) problem validates that the MOGWO algorithm can solve any kind of non-linear and complex problem with many constraints in unknown search space [17], [18], [19].

Meanwhile, special emphasis is being paid to incorporating renewable energy supplies into the grid to decarbonize the electric power system. Solar photovoltaic and wind deployments are continuously rising due to concerns about global warming due to climate change. On the alternative, fossil fuel-based power generation systems are becoming less adaptable. According to recent research, dynamic energy supplies such as solar and wind have characteristics that span several time scales, impacting various layers of power system regulation. Such results indicate that, as RES adoption grows, standard load flow analyses aren't adequate to assure dependability through efficient utilization of resources. It is also proven that, due to the high integration of RESs, operators have difficulties in handling power requirements and depend on user curtailment. Furthermore, the unpredictability and intermittent nature of fluctuating energy sources are expected to raise backup capacity needs, hence raising the incremental cost of electricity [20], [21], [22].

Different alternatives have already been dedicated to the OPF problems for the last few decades. To handle the hydrothermal OPF, the authors of [23] have utilized nonlinear and linear programming methods. The OPF with continuous and discrete optimization parameters was solved using a mixed Particle Swarm Optimization (PSO) algorithm [24]. For the OPF problem with integrated security restrictions, the authors of [25] presented a PSO with reconstructive operators. The authors of [26] have solved the OPF problem using PSO with aging challengers and leaders. The OPF problem was optimized using glowworm swarm optimization in [27], using the minimization of emission and generation cost as fitness functions. To handle the OPF effectively, the authors of [28] have devised an enhanced colliding bodies optimizer. The Differential Evolutionary (DE) algorithm for single- and multi-objective optimal power flow problems was given in Ref. [29]. For the OPF problem, the authors of [30] have presented an enhanced Artificial Bee Colony (ABC) algorithm based on orthogonal learning. To overcome the limited OPF challenge, the authors of [31] have proposed a unique moth swarm method. Upgraded self-adaptive DE with a mixed crossover algorithm was used to address multi-objective OPF problems with conflicting objectives [32]. To obtain OPF solutions, the authors in [33] and [34] used a DE algorithm combined with effective constraint handling strategies. The authors of [35] have presented an enhanced social spider optimizer for tackling the optimal power flow problem with a single objective. The authors of [36] suggested an adaptive perturbation-guiding JAYA algorithm developed to deal with various single-objective optimal power flow problems. Although these algorithms have produced more satisfactory outcomes, the majority of such algorithms are based on conventional thermal-based power generation units and ignore other essential objectives, such as emission reduction of toxic gases, such as CO_2, NO_x, and SO_x in ton/hr.

Since the citations above consider traditional generation units, some articles now consider an electrical system combining wind and coal-based power units in their quest for the lowest generating prices. The authors of [37] presented

the Gbest-directed ABC to increase OPF results reported in previous studies using the same experimental design. In the OPF problem, the authors of [38] proposed an Improved Bacteria Foraging Algorithm (IBFA) and a framework for a double-fed induction generator to emphasize restrictions on the ability to create VAR fuel. The STATCOM is another VAR power compensating device for a network with coal-based and wind units (static synchronous compensator). Ant colony optimization and IBFA were also used to tackle the OPF problem [39]. The authors of [40] suggested a method for assessing wind power prices. The difficulty of planning generators for ELD is common for a grid with both coal-based and wind units. The random nature of the wind power output was provided by [41]. Researchers in [42] also used the DFIG wind turbine model despite solving a comparable problem. The complex ELD problem, which included a wide variety of wind energy and risk reserve constraints, was discussed in [43]. The authors of [44] have incorporated the valve-point loading impact in the Dynamic ELD (DELD) structure of the producing unit and emanation. The optimal power flow scheduling approach is given in [45] for a single system with battery energy storage, Photovoltaic (PV), and gas-based power generation units. The authors of [46] defined pumped hydro storage as a storage alternative for a freestanding hybrid network comprising a wind turbine, solar PV unit, and a diesel generator. The problem was developed using three sources, as mentioned in ref. [47], in addition to a single objective DELD problem. The authors of [48] have used non-conventional sources such as coal-based and solar-wind power, as well as battery storage, to achieve optimum scheduling. Biswas *et al.* [34] established a framework for evaluating OPF challenges for solar, wind, and river units with various probability density functions.

Even though incorporating renewable energy resources into OPF is addressed in such literature, it should have been viewed as a starting point rather than an end. Numerous literature reviews examine a single optimization objective when addressing the OPF problem with renewable energy. Other objectives, especially those related to emissions, are significant and, therefore, should be considered. In conclusion, multi-objective OPF with renewable energy sources merits further investigation. The typical IEEE-30 bus system is enhanced in this research by incorporating probabilistic wind and solar energy. Sustainable energy generators, like traditional power generators, are now aiming to emphasize everyday research more. In addition to coal-based units, solar, wind, and small-hydro power generation units are considered in this paper, and the OPF problem is handled by both single- and multi-objective algorithms. For research purposes, these sustainable energy sources are being integrated into the standard IEEE 30-bus network. The Equilibrium Optimizer (EO) technique can be used to generate clusters of solutions for single-objective and multi-objective problems [49], [50]. The Multi-Objective Whale Optimization Algorithm (MOWOA) is developed by equipping the whale optimization algorithm with a crowding distance, an archive, and whales' position (according to ranking) selection method based on Pareto optimal dominance nature.

The MOWOA algorithm is first applied on 17 standard test functions (including eight unconstraint, five constraints, and four engineering design multi-objective problems) to prove its capability in terms of qualities and quantities showing numerical as well as convergence and coverage of Pareto optimal front with respect to true Pareto front. Then, after the MOWOA algorithm is applied to a real-world complex MOOPF problem, the algorithm is proved with a Summation-based Multi-Objective DE (SMODE) algorithm, Multi-Objective Symbiotic Search Algorithm (MOSOS), Multi-Objective Colliding Bodies Optimization (MOCBO) algorithm, Multi-Objective PSO (MOPSO), Non-Dominated Sorting Genetic Algorithm (NSGA-II), and other well-known algorithms in the field of multi-objective algorithms. A storage and leader selection strategy were then combined into a single objective Ion Motion Optimization (IMO) approach to solving multiobjective problems. A group of unconstrained, constrained, and engineering benchmark functions were employed to assess the performance of the Multi-Objective IMO (MOIMO) [51], [52], [53], [54], [55], [56], [57], [58], [59], [60], [61]. The outcomes of MOIMO are compared with those of the Multi-Objective Dragonfly Algorithm (MODA), Multi-Objective Multi-Verse Optimizer (MOMVO), and Multi-Objective Ant Lion Optimizer (MOALO). It was evident that the MOIMO algorithm is very competent and modest in determining an exact estimation of the Pareto optimal front with uniform dispersal across considered objectives with minimum simulation time. The major contributions of this paper are as follows.

- Formulation of objective functions for OPF problem with single- and multi-objective to handle four objective functions, such as minimization of total fuel cost, voltage deviation, voltage stability index, and the active power loss
- Development and application of single- and Multi-Objective Equilibrium Optimizer (MOEO) in OPF problem of hybrid power network considering the security constraints
- Application of suitable Probability Density Functions (PDFs) to randomize the behavior of solar PV, wind, and small hydro plants
- Validating the suggested algorithm on a modified IEEE-30 bus hybrid power system network
- Comparative analysis is made among well-established algorithms

The paper is organized as follows. Section 2 describes the mathematical models that present the uncertainty in solar-wind-small hydro energy outputs in the context of the OPF problem. Section 3 clarifies the various objective functions. Section 4 describes the EO and MOEO algorithms and their application in the OPF problem. The quantitative findings and analysis are found in Section 5, while the concluding remarks are found in Section 6.

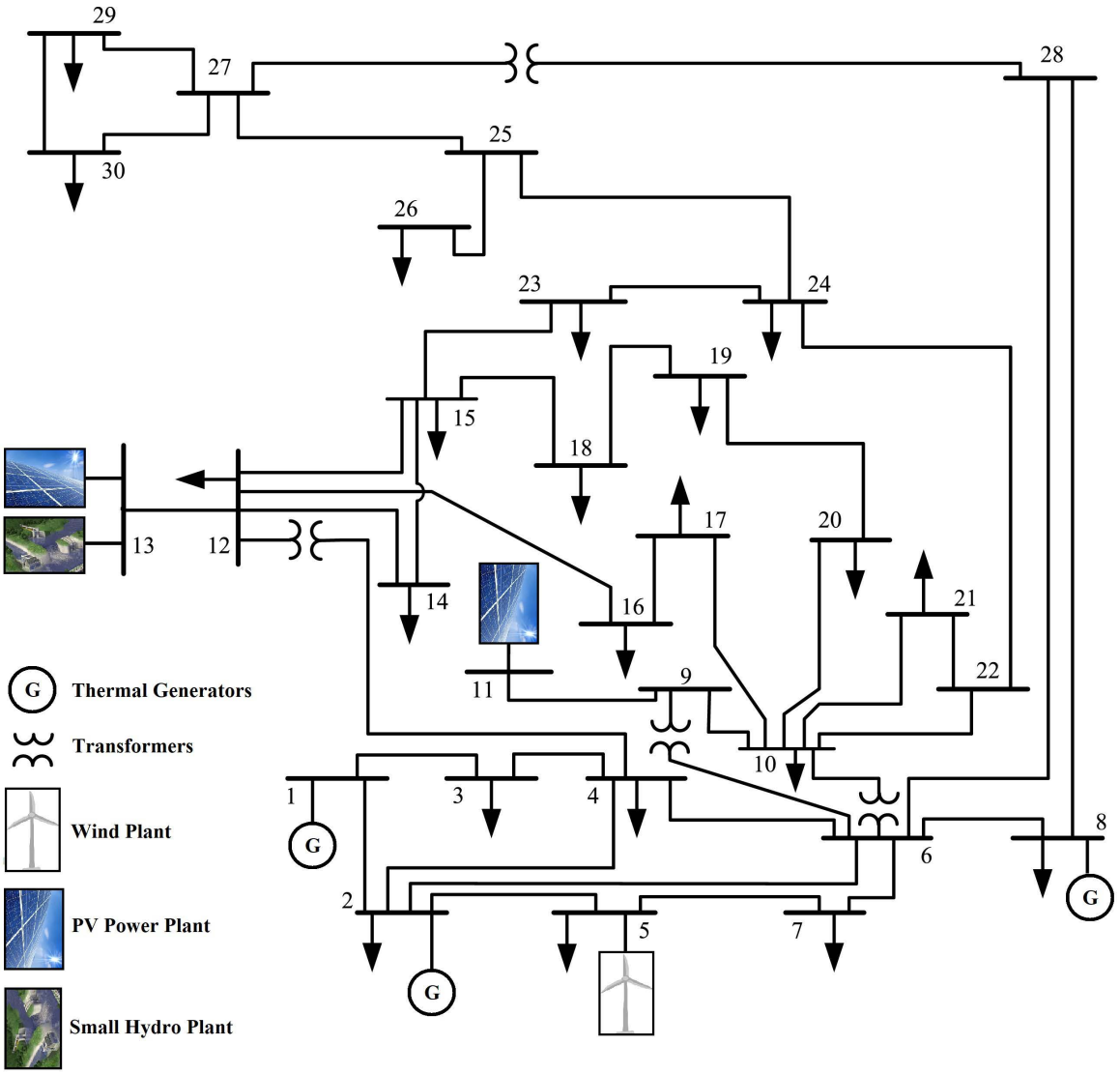

FIGURE 1. Enhanced IEEE 30-bus hybrid wind-solar-small hydroelectric power plant system [34].

TABLE 1. Key specification of the system of the hybrid network considered in this paper [34].

Items	Quantity	Ratings
Buses	30	[34]
Branches	41	[34]
Coal-based Generators	3	Buses: 1 (swing), 2 and 8
PV generator	1	Bus-11
Hybrid unit	1	Bus-13
Wind generator	1	Bus-5
Bus voltage (Load)	24	Between 0.95 p.u. to 1.05 p.u.
Load	-	126.2 MVAr, 283.4 MW
Control vectors	11	Five generators scheduled real power, six generator bus voltages

TABLE 2. Upper Bound (UB) and Lower Bound (LB) of control parameters [34].

Variables	UB	LB	Variables	UB	LB
PG2 (MW)	80	20	V11 (p.u.)	1.10	0.95
PG3 (MW)	35	10	V13 (p.u.)	1.10	0.95
PG4 (MW)	75	0	PG1 (MW)	140	30
PG5 (MW)	60	0	QG1 (MVAr)	150	−20
PG6 (MW)	50	0	QG2 (MVAr)	60	−20
V1 (p.u.)	1.10	0.95	QG3 (MVAr)	40	−15
V2 (p.u.)	1.10	0.95	QG4 (MVAr)	35	−30
V5 (p.u.)	1.10	0.95	QG5 (MVAr)	30	−25
V8 (p.u.)	1.10	0.95	QG6 (MVAr)	25	−20

II. MATHEMATICAL MODEL

This paper considers the enhanced IEEE-30 bus network to validate the performance of the EO and MOEO when it handles the OPF problem. The power framework of the improved IEEE-30 bus system is shown in Fig. 1, where thermal units are located at buses 1, 2, and 8, one solar PV unit is located at bus 11, one wind unit is located at bus 5, and one small hydro with hybrid PV unit is located at bus 13. Table 1 summarizes a complete specification of the selected

TABLE 3. Emission and cost coefficients of the system considered in this paper.

Generators	Bus Number	a	b	c	d	e	α	β	γ	ω	μ
TG1	1	30	2	0.00375	18	0.037	4.091	-5.554	6.49	0.0002	6.667
TG2	2	25	1.75	0.0175	16	0.038	2.543	-6.047	5.638	0.0005	3.333
TG3	8	20	3.25	0.00834	12	0.045	5.326	-3.55	3.38	0.002	2

IEEE-30 bus power system. Table 2 shows the upper and lower bounds of the selected power system.

A. GENERATION COST OF THERMAL UNITS

As discussed in the literature, there are general optimization objectives, namely, minimizing the generating cost, the active power loss, and the voltage deviation. In classical coal-based power generation, the cost is computed as follows, allowing the valve-point loading effect.

$$C_T\left(P_{TG}\right) = \sum_{i=1}^{N_{TG}} a_i + b_i P_{TGi} + c_i P_{TGi}^2 + \left| d_i \times sin\left(e_i \times \left(P_{TGi}^{min} - P_{TGi}\right)\right)\right| \quad (1)$$

where a_i, b_i, and c_i denote the cost coefficients for i^{th} generator, and d_i and e_i denote the cost constants for i^{th} generator with a loading effect. The values of the emission and cost coefficients are presented in Table 3.

B. EMISSION

Minimizing emissions is an extremely important challenge. One main reason is that typical thermal power generation units release toxic gases, such as CO_2, NO_x, and SO_x, into the atmosphere, leading to pollution. The emission in tons/hour can be computed as follows.

$$\text{Emission}, E = \sum_{i=1}^{N_{TG}} \left[\left(\alpha_i + \beta_i P_{TGi} + \gamma_i P_{TGi}^2\right) \times 0.01 + \omega_i e^{(\mu_i P_{TGi})}\right] \quad (2)$$

where, α_i, β_i,γ_i, ω_i and μ_i are the emission constants of the i^{th} unit and the values of such coefficients are listed in Table 3.

C. DIRECT COSTS OF STOCHASTIC UNITS

The direct cost associated with the wind unit is mathematically modeled with the P_{ws} scheduled power from the same sources. The associated cost is as follows.

$$C_w\left(P_{ws}\right) = g_w \times P_{ws} \quad (3)$$

where, g_w signifies the direct cost coefficient and P_{ws} signifies the scheduled wind power. Likewise, the direct cost associated with the photovoltaic unit is presented with the P_{ss} scheduled power from the same sources. The associated cost is presented as follows.

$$C_s\left(P_{ss}\right) = h_s \times P_{ss} \quad (4)$$

where, h_s signifies the direct cost coefficient and P_{ss} signifies the scheduled PV power. A hybrid solar unit with a small-hydro unit is known as a third sustainable energy source. So, the scheduled power consists of the summation of the hydropower and the PV output power. The direct costs for the PV and the small-hydro units are as follows.

$$C_s\left(P_{ss}\right) = C_s\left(P_{ssh,h} + P_{ssh,s}\right) = P_{ssh,s} \times h_s + P_{ssh,h} \times m_s \quad (5)$$

where, P_{ss} denotes the expected production from the hybrid plant, $P_{ssh,s}$ denotes the influence of the PV unit, and $P_{ssh,h}$ denotes the influence of the small-hydro unit. The direct variables of price h_s and m_s are similar to the previous discussion.

D. UNCERTAIN SUSTAINABLE WIND POWER COST

The standby cost for the wind unit is formulated as follows.

$$C_{Rw}\left(P_{w,s} - P_{w,av}\right) = K_{Rw}\left(P_{w,s} - P_{w,av}\right) = K_{Rw}\int_0^{P_{ws}} f_w\left(p_w\right)\left(P_{w,s} - p_w\right) dp_w \quad (6)$$

where, K_{Rw} denotes the reserve cost coefficient for wind component, the wind power Probability Density Function (PDF) is represented by $f_w\left(p_w\right)$, and $P_{w,s}$ denotes the amount of power that is accessible from the same wind unit. The penalty cost for the same is given as follows.

$$C_{Pw}\left(P_{w,av} - P_{w,s}\right) = K_{Pw}\left(P_{w,av} - P_{w,s}\right) = K_{Pw}\int_{P_{ws}}^{P_{wr}} f_w\left(p_w\right)\left(p_w - P_{w,s}\right) dp_w \quad (7)$$

where, P_{wr} signifies the rated output from the wind unit and K_{Pw} denotes the wind penalty cost coefficient.

E. UNCERTAIN SUSTAINABLE PV POWER COST

The standby cost of a solar PV unit can be written as follows.

$$C_{Rs}\left(P_{s,s} - P_{s,av}\right) = K_{Rs}\left(P_{s,s} - P_{s,av}\right) = f_s\left(P_{s,av} < P_{s,s}\right) \times K_{Rs} \times \left[P_{s,s} - E\left(P_{s,av} < P_{s,s}\right)\right] \quad (8)$$

where, K_{Rs} denotes the standby price constant regarding solar PV units, $P_{s,av}$ denotes the amount of power that is accessible from the same PV unit, $f_s(P_{s,av} < P_{s,s})$ represents the probability of PV output shortage rate concerning scheduled output power $P_{s,s}$, and $E(P_{s,av} < P_{s,s})$ represents the expected PV output power lesser than $P_{s,s}$. The penalty price for overrating PV units can be given as follows.

$$C_{Ps}\left(P_{s,av} - P_{s,s}\right) = K_{Ps}\left(P_{s,av} - P_{s,s}\right) = K_{Ps} \times f_s\left(P_{s,av} > P_{s,s}\right) \times \left[E\left(P_{s,av} > P_{s,s}\right) - P_{s,s}\right] \quad (9)$$

TABLE 4. PDF constants of solar PV, wind, and small hydro plants [34].

Wind Unit					PV Unit		
Wind #	Total Turbines (3MW each)	Weibull mean, M_{wbl}	Weibull parameters	Rated power P_{wr} (MW)	Lognormal mean, M_{lgn}	Lognormal parameters	Rated power P_{sr} (MW)
Bus-5	25	$v = 7.976$ m/s	$k = 2, c = 9$	75	G=483W/m^2	$\mu = 5.2$ σ= 0.6	50 Bus-11
Hybrid Solar +Small Hydro (Bus-13)							
PV-rated power, P_{sr} (MW)	Lognormal PDF parameters	Small-Hydro rated power, P_{hr} (MW)	Gumbel PDF parameters	Bus-5 wind unit Bus-11 PV unit Bus-13 Hybrid PV + Small hydro unit			
45 (bus-13)	μ = 5.0 σ= 0.6	5	λ = 15 γ= 1.2				

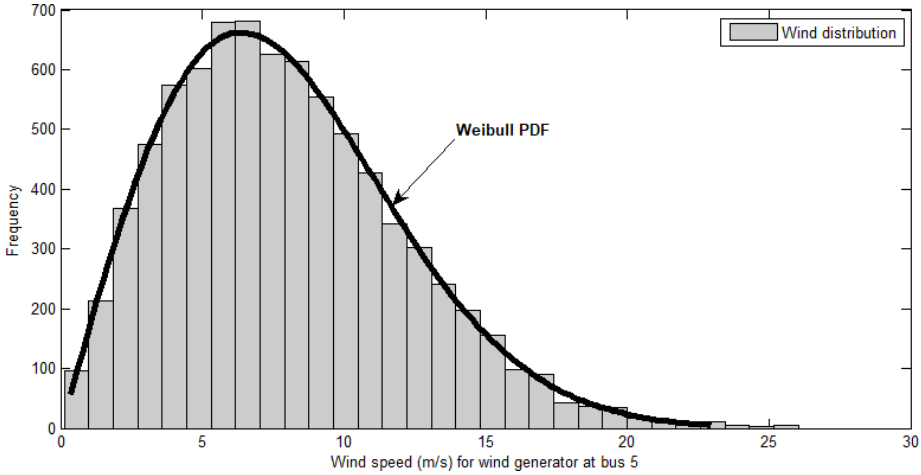

FIGURE 2. Weibull function for a wind plant at bus-5.

where, K_{Ps} represents the coefficient of penalty price regarding SPV unit, $f_s(P_{s,av} > P_{s,s})$ represents the expected PV output in excess of the scheduled output, and $E(P_{s,av} > P_{s,s})$ represents the expected PV output higher than $P_{s,s}$.

F. UNCERTAIN SUSTAINABLE HYBRID SOLAR PV AND SMALL-HYDRO POWER COST

In this subsection, another sustainable generation network is a cluster of small-scale hydropower units, and solar PV units are considered. The water flow strength determines the generation of the small-hydro unit that is famous for accompanying Gumbel distribution [41]. Satisfying Eq. (8), the reserve cost for hybrid unit output is as follows.

$$\begin{aligned} C_{Rsh}\left(P_{ssh} - P_{shav}\right) &= K_{Rsh}\left(P_{ssh} - P_{shav}\right) \\ &= K_{Rsh} \times f_{sh}\left(P_{shav} < P_{ssh}\right) \\ &\quad \times \left[P_{ssh} - E\left(P_{shav} < P_{ssh}\right)\right] \end{aligned} \tag{10}$$

where, K_{Rsh} is the standby cost coefficient and is related to the hybrid unit and P_{shav} is the actual accessible output from the system. The possibility of a shortage of hybrid system output from the scheduled power (P_{ssh}) is given by $f_{sh}(P_{shav} < P_{ssh})$ and the principle of distributed power below P_{ssh} is $E(P_{shav} < P_{ssh})$. After Eq. (9), the cost of penalty for underestimating the performance of the hybrid system is as follows.

$$\begin{aligned} C_{Psh}\left(P_{shav} - P_{ssh}\right) &= K_{Psh}\left(P_{shav} - P_{ssh}\right) \\ &= K_{Psh} \times f_{sh}\left(P_{shav} > P_{ssh}\right) \\ &\quad \times \left[E\left(P_{shav} > P_{ssh}\right) - P_{ssh}\right] \end{aligned} \tag{11}$$

where, K_{Psh} is the penalty cost coefficient is related to the hybrid unit, $f_{sh}(P_{shav} > P_{ssh})$ is the possibility of the excess of hybrid system power from the scheduled power (P_{ssh}) , and$E(P_{shav} > P_{ssh})$ is the expectancy of the hybrid system output above P_{ssh}.

G. UNCERTAINTY OF STOCHASTIC SOLAR/WIND/SMALL-HYDRO UNITS

Wind speed distributions are represented using the Weibull Probability Density Function (PDF). The following is how the Weibull PDF was used by the authors of [34] to depict the probability of wind speed in meters per second. The data of the suggested Weibull scale (c) and shape (k) constants were presented in Table 4. The distributions of the Weibull curve and wind frequency are shown in Fig. 2 by taking 8000 steps from the Monte-Carlo simulation.

The probability of Weibull PDF following wind velocity vm/s, including scale factor (c) and shape factor (k) could be

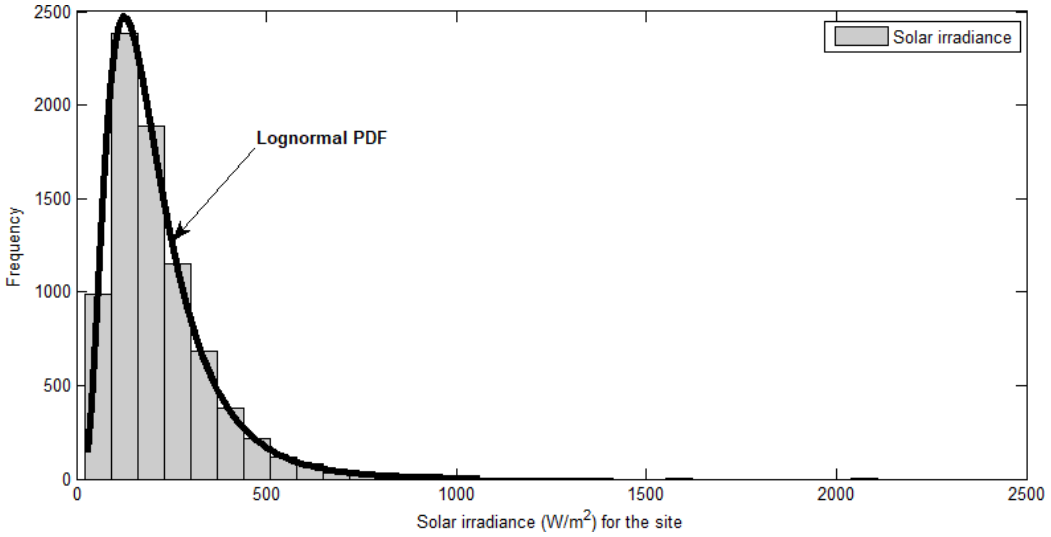

FIGURE 3. Lognormal function for the PV unit at bus-11.

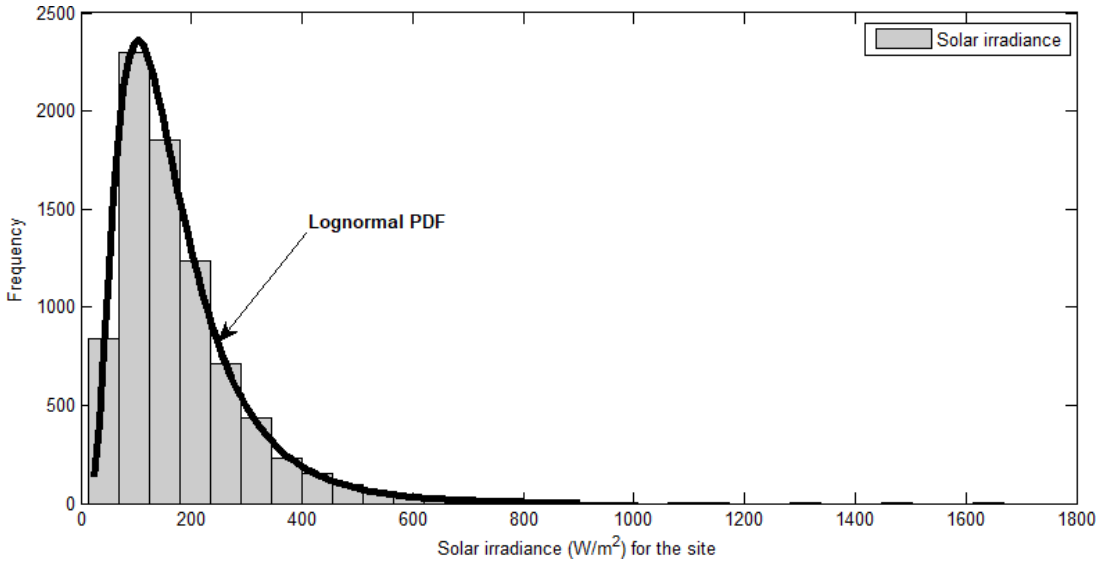

FIGURE 4. Lognormal PDF for the solar irradiance distribution for solar PV plant located at bus-13 (Solar hybridized with a small-hydro plant).

estimated as follows.

$$f_v(v) = \left(\frac{k}{c}\right)\left(\frac{v}{c}\right)^{(k-1)} e^{-\left(\frac{v}{c}\right)^k}, \quad \text{for } 0 < v < \infty \quad (12)$$

The Weibull distribution mean is reported as follows.

$$M_{wbl} = c * \Gamma\left(1 + k^{-1}\right) \quad (13)$$

The expression for $\Gamma(x)$ is presented as follows.

$$\Gamma(x) = \int_0^{\infty} e^{-t} t^{x-1} dt \quad (14)$$

The thermal plant at bus-11 of the standard IEEE-30 bus system is replaced with the PV unit. The power production of the PV unit is contingent on sun irradiation (G) that follows the Lognormal PDF [34]. The solar irradiation probability tracking Lognormal PDF has a standard deviation σ and mean μ can be presented as follows.

$$f_G(G) = \frac{1}{G\sigma\sqrt{2\pi}} exp\left\{\frac{-(lnx - \mu)^2}{2\sigma^2}\right\}, \quad \text{for } G > 0 \quad (15)$$

By replicating the Monte-Carlo setup with a set point of 8000, Figure 3 defines a frequency distribution and Lognormal distribution of solar irradiation. The mean of the Lognormal distribution is given as follows.

$$M_{lgn} = exp\left(\mu + \frac{\sigma^2}{2}\right) \quad (16)$$

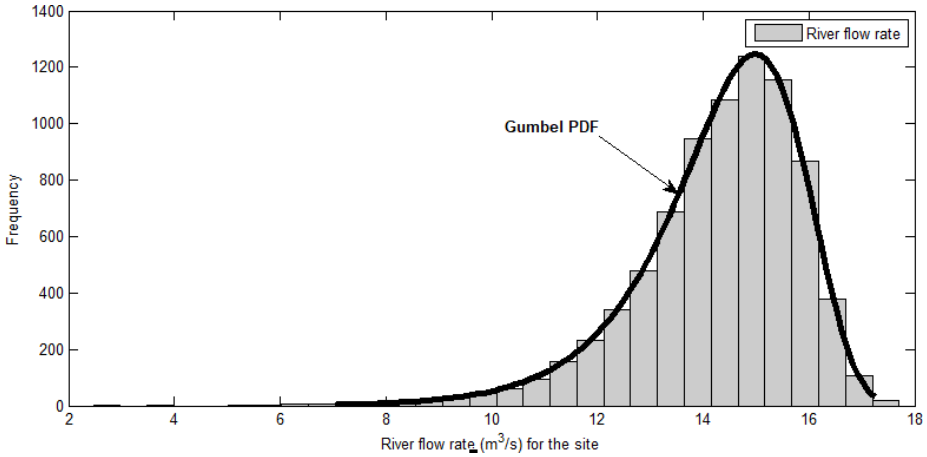

FIGURE 5. Gumbel PDF for river flow rate distribution located at bus-13 (Solar with a small-hydro plant).

TABLE 5. Price coefficients for sustainable energy resources.

Coefficient of Direct Expense ($/MW)			Price Coefficient of Reserve ($/MW)			Penalty coefficient of price ($/MW)		
Wind (bus-5)	PV (bus-13 & 11)	Hybrid plant (bus-13)	Wind (bus-5)	PV (bus-11 & 13)	Hybrid plant (bus 13)	Wind (bus-5)	PV (bus-11 & 13)	Hybrid plant (bus-13)
$g_w = 1.7$	$h_s = 1.6$	$m_h = 1.5$	$K_{Rw} = 3$	$K_{Rs} = 3$	$K_{Rsh} = 3$	$K_{Pw} = 1.4$	$K_{Ps} = 1.4$	$K_{Psh} = 1.4$

The possibility of water flow rate Q_w, subsequent Gumbel PDF through position constant λ and scale constant γ has been written as follows.

$$f_Q(Q_w) = \frac{1}{\gamma}\exp\left(\frac{Q_w - \lambda}{\gamma}\right)\exp\left[-\exp\left(\frac{Q_w - \lambda}{\gamma}\right)\right] \quad (17)$$

The hybrid PV and hydropower unit are at bus-13 of the enhanced network, swapping the coal-based generator. Fig. 4 shows the solar PV PDF output and Lognormal scale obtainable for the PV located at bus-13. Figure 5 illustrates the strength of water mass flow distribution and the scale of Gumbel. To perform an 8000 Monte Carlo setup, both figures are generated using the basic standards of PDF parameters tabulated in Table 4.

H. POWER MODELS OF SOLAR PV, WIND, AND HYBRID PLANTS

The wind plant at bus-5 comprised the combined outputs of the 25 turbines. The power capacity of each turbine is 3 MW. Depending on the speed, the exact energy production of the wind turbine varies. In terms of wind velocity (v), the turbine output power is expressed as follows.

$$p_w(v) = \begin{cases} p_{wr}, & \text{for } v_r < v \le v_{out} \\ 0, & \text{for } v < v_{in} \text{ and } v > v_{out} \\ p_{wr}\left(\frac{v - v_{in}}{v_r - v_{in}}\right), & \text{for } v_{in} \le v \le v_r \end{cases} \quad (18)$$

where, v_{out}, v_r, and v_{in}, denotes the cut-out, rated, and cut-in speed of the wind turbine, respectively and p_{wr} signifies the rated generated power of the turbine. The Enercon E82-E4 model datasheet is referenced for the 3MW wind turbine. The different speeds are $v_{out} = 25$ meter/sec, $v_r = 16$ meter/sec, and $v_{in} = 3$ meter/sec. The solar irradiation $P_s(G)$ to transform the energy of the photovoltaic can be represented as follows.

$$P_s(G) = \begin{cases} P_{sr}\left(\frac{G^2}{G_{std}R_c}\right), & \text{for } 0 < G < R_c \\ P_{sr}\left(\frac{G}{G_{std}}\right), & \text{for } G \ge R_c \end{cases} \quad (19)$$

where, R_c denotes a particular irradiance position set as 120 W/m^2, G_{std} denotes the solar irradiation in the typical environment fixed at 1000 W/m^2, and the PV unit's rated performance is P_{sr}. The flow rate of water (Q_w) and effective pressure head (H_w) are calculated by the output of a small hydro plant. The efficiency of the small hydro plant can therefore be determined as follows.

$$P_H(Q_w) = \eta\rho g Q_w H_w \quad (20)$$

where η stands for the efficiency of the generator-turbine set, g denotes the acceleration due to gravity, and ρ denotes the water concentration. To calculate the hydro output, the parameters are set at these values, η =0.85, ρ =1000 kg/m^3, $g = 9.81\ m/s^2$, and H_w =25 m. Table 5 shows the quantitative value of direct, penalty, and reserve cost factors for wind, PV, and small hybrid hydropower. The direct cost factors are set, so that wind energy is the most priced, trailed by PV

power and hydroelectric power. The reserve cost coefficient is larger than the direct cost coefficient for sustaining spinning reserves. On the other hand, the penalty for not using the power available is less than the direct cost.

III. PROBLEM FORMULATION

The optimal VAR power and real power dispatch objectives are included in the OPF. The following objectives for OPF with PV, wind, and hybrid plants are included in this section. Entirely the fitness functions considered in this paper are minimization functions.

A. MINIMIZATION OF TOTAL FUEL COST (TFC)

The very first objective is the reduction of the total overall cost. Including coal-based unit prices and direct, reserve, and penalty prices for non-conventional resources is the expense of the entire generation. Therefore, the combined price for a coal-based power plant, a wind power plant, a solar photovoltaic power plant, and a hybrid solar and small hydropower plant is presented as follows.

$$\begin{aligned} f1 = C_{Tot} &= C_T\left(P_{TG}\right) \\ &+ \left[C_w\left(P_{ws}\right) + C_{Rw}\left(P_{ws} - P_{wav}\right) + C_{Pw}\left(P_{wav} - P_{ws}\right)\right] \\ &+ \left[C_s\left(P_{ss}\right) + C_{Rs}\left(P_{ss} - P_{sav}\right) + C_{Ps}\left(P_{sav} - P_{ss}\right)\right] \\ &+ \left[C_{sh}\left(P_{ssh}\right) + C_{Rsh}\left(P_{ssh} - P_{shav}\right)\right. \\ &\left. + C_{Psh}\left(P_{shav} - P_{ssh}\right)\right] \end{aligned} \tag{21}$$

B. VOLTAGE DEVIATION (VD) MINIMIZATION

The VD is a measure of voltage reliability of entire load buses in the system. The voltage variations of the PQ bus can be controlled starting at 1.0 for every unit, resulting in a more consistent voltage profile overall. The problem is formulated as follows.

$$f2 = VD = \sum_{i=1}^{N_{pq}} |v_i - 1| \tag{22}$$

where v_i represents the voltage level of i^{th} bus in p.u. and N_{pq} presents the number of PQ buses.

C. MINIMIZATION OF ACTIVE POWER LOSS (APL)

Transmission line losses are caused by the transmission cables' due to their resistive nature. When electrical energy flows from one node to the other in a branch, it dissipates as heat. Whenever this loss is incurred, it impacts the node voltages, which may be explained in terms of the magnitude and angle of the node voltage. The third objective function for minimizing transmission network Active Power Loss (APL) can be represented as follows.

$$f3 = APL = P_{LOSS} = \sum_{i=1}^{NB} P_{Gi} - \sum_{i=1}^{NB} P_{Di} \tag{23}$$

where, P_{Gi} and P_{Di} denote the generated power output and power distributed at i^{th} bus, and NB denotes the number of buses.

D. VOLTAGE STABILITY INDEX (L-INDEX)

The L-index, which depicts each bus's voltage uniformity margins, is the most important metric for keeping the constant voltage at a tolerable level under typical conditions. L-index provides a scalar count for any PQ bus. The L-index remains between '0' (no load) and '1' (maximum load) (collapse of voltage). The total voltage collapse indication for the i^{th} bus is as follows.

$$L_j = \left|1 - \sum_{i=1}^{N_g} F_{ji} \frac{V_i}{V_j}\right|, \quad \forall j = 1, 2, \ldots, NL \tag{24}$$

$$F_{ji} = -\left[Y_2\right]\left[Y_1\right]^{-1} \tag{25}$$

where Y_2 and Y_1 denote the sub-matrices of Y_{BUS}. The fitness function to improve stability is described as follows.

$$f4 = L = \max\left(L_j\right) \quad \forall j = 1, 2, \ldots, NL \tag{26}$$

E. EQUALITY CONSTRAINTS

The power flow expressions provide equality constraints, showing that both reactive and real power generated in a network necessity satisfy the system's power demands and losses.

$$Q_{Gi} - Q_{Di} - V_i \sum_{j=1}^{NB} V_j \left[G_{ij} \sin\left(\delta_{ij}\right) - B_{ij} \cos\left(\delta_{ij}\right)\right] = 0 \quad \forall\, i \in NB \tag{27}$$

$$P_{Gi} - P_{Di} - V_i \sum_{j=1}^{NB} V_j \left[G_{ij} \cos\left(\delta_{ij}\right) + B_{ij} \sin\left(\delta_{ij}\right)\right] = 0 \quad \forall\, i \in NB \tag{28}$$

where NB signifies the total buses, P_{Di} and Q_{Di} signify the real power and reactive power demand at i^{th} bus, $\delta_{ij} = \delta_i - \delta_j$ denotes the variance in phase angles of voltage among bus i and bus j, and P_{Gi} and Q_{Gi} are the active power and reactive power generation respectively of i^{th} bus by either unit (coal-based or renewable) as appropriate. G_{ij} displays the conductance and B_{ij} signifies the susceptance among bus j and bus i, correspondingly.

F. INEQUALITY CONSTRAINTS

The functional limitations of systems, as well as the security limits of lines and PQ buses, constituted inequity constraints. The following are the generator boundaries:

$$P_{TGi}^{min} \le P_{TGi} \le P_{TGi}^{max} \quad \forall i \in N_{TG} \tag{29}$$

$$P_{\text{ws}}^{min} \le P_{ws} \le P_{\text{ws}}^{max} \tag{30}$$

$$P_{ss}^{min} \le P_{ss} \le P_{ss}^{max} \tag{31}$$

$$P_{ssh}^{min} \le P_{ssh} \le P_{ssh}^{max} \tag{32}$$

$$Q_{TGi}^{min} \le Q_{TGi} \le Q_{TGi}^{max} \quad \forall i \in N_{TG} \tag{33}$$

$$Q_{\text{ws}}^{min} \le Q_{ws} \le Q_{\text{ws}}^{max} \tag{34}$$

$$Q_{ss}^{min} \le Q_{ss} \le Q_{ss}^{max} \tag{35}$$

$$Q_{ssh}^{min} \le Q_{ssh} \le Q_{ssh}^{max} \tag{36}$$

$$V_{Gi}^{min} \le V_{Gi} \le V_{Gi}^{max}, \quad i = 1, \ldots, NG \tag{37}$$

Security bounds are as follows

$$V_{L_p}^{min} \leq V_{L_p} \leq V_{L_p}^{max}, \quad p = 1, \ldots..,NL \tag{38}$$

$$S_{l_q} \leq S_{l_q}^{max}, \quad q = 1, 2, \ldots, nl \tag{39}$$

The active power output limits of coal-based, PV, and wind units are denoted by Eq. 29-32. The reactive power of generating units is then represented by Eq. 33-36. The entire voltage control buses are depicted in *NG*. Equation 37 depicts voltage bounds for PV buses, whereas Eq. 38 depicts voltage boundaries for PQ buses and *NL* denotes the total PQ buses. For the total *nl* lines in a network, Eq. 39 is used to establish line loading boundaries.

IV. SINGLE- AND MULTI-OBJECTIVE EQUILIBRIUM OPTIMIZER

This part describes the elementary notion of the single-objective equilibrium optimizer and the Multi-Objective Equilibrium Optimizer (MOEO) formulation.

A. EQUILIBRIUM OPTIMIZER (EO)

Equilibrium Optimizer is a metaheuristic optimization tool that was reported by Faramarzi *et al.* [49]. The strategy is based on mass conservation balances for a particle entering and departing a regulated volume, to achieve equilibrium. The optimization procedure, likewise, tries to maintain the system's balance. There are three primary mathematical representations, i) initializing concentrations, ii) computing an equilibrium pool of candidates, and iii) updating concentrations. The mathematical model of the EO algorithm is discussed in this sub-section. The readers should read the base paper for comprehensive details [49]. Like entirely other metaheuristic algorithms, the initial random population solution of EO is generated using Eq. 40.

$$C_i^{\text{initial}} = C_{min} + rand_i \left(C_{max} - C_{min}\right) \quad i = 1, 2, \ldots, n \tag{40}$$

where n denotes the number of particles in the population, C_i^{initial} signifies the initial concentration vector, C_{min} and C_{max} are the lower and upper bounds, and $rand_i$ is a random number between [0,1]. The best solution is to metaphorically reach an equilibrium condition by calculating candidate solutions and the equilibrium pool. To reach the unknown equilibrium state, the EO uses five concentrations. The particle pool is made up of the average of the four best concentrations so far. The following are the pool's characteristics.

$$\overrightarrow{C}_{eq,pool} = \left\{\overrightarrow{C}_{eq(1)}, \overrightarrow{C}_{eq(2)}, \overrightarrow{C}_{eq(3)}, \overrightarrow{C}_{eq(4)}, \overrightarrow{C}_{eq(ave)}\right\} \tag{41}$$

Equation 42 is used to update the population solution in EO.

$$\overrightarrow{C} = \overrightarrow{C}_{eq} + \left(\overrightarrow{C} - \overrightarrow{C}_{eq}\right).\overrightarrow{F} + \frac{\overrightarrow{G}}{\overrightarrow{\lambda}}\left(1 - \overrightarrow{F}\right) \tag{42}$$

$$\overrightarrow{F} = e^{-\overrightarrow{\lambda}(t-t_0)} \tag{43}$$

$$t = \left(1 - \frac{FE}{Max\_FEs}\right)^{\left(a_2\left(\frac{FE}{Max\_FEs}\right)\right)} \tag{44}$$

where *Max_FEs* denotes the total number of function evaluations, and *FE* is the current function evaluations.

$$\overrightarrow{t}_0 = \frac{1}{\overrightarrow{\lambda}} ln\left(-a_1 sign(\overrightarrow{r} - 0.5)\left[1 - e^{-\overrightarrow{\lambda} t}\right]\right) + t \tag{45}$$

$$\overrightarrow{G} = \overrightarrow{G}_0 e^{-\overrightarrow{\lambda}(t-t_0)} \tag{46}$$

$$\overrightarrow{G}_0 = \overrightarrow{RCP}\left(\overrightarrow{C_{eq}} - \overrightarrow{\lambda}\,\overrightarrow{C}\right) \tag{47}$$

$$\overrightarrow{RCP} = \begin{cases} 0.5r_1, & r_2 \geq RP \\ 0, & \text{Otherwise} \end{cases} \tag{48}$$

where $r1$, $r2$, and r are arbitrary numbers $\in$ [0, 1], and $r1$ and $r2$ are factors that balance the exploitation and exploration phase of EO. The term sign $(\overrightarrow{r} - 0.5)$ regulates the exploitation and exploration directions. The rate $\overrightarrow{G}$ is a section that may progress the divergence procedure and $\overrightarrow{RCP}$ controls if the control variable is utilized or not in the updating procedure.

B. MULTI-OBJECTIVE EQUILIBRIUM OPTIMIZER

In multiobjective problems, two or more objective functions are solved at the same time when entirely constraints are satisfied [51], [52], [53]. To describe the multi-objective OPF problem, several optimization approaches are used in the literature. From the previous works, it can be seen that many researchers have turned a multiobjective problem into a single-objective problem by combining the two conflicting objective works into a single-objective problem and then employing the weighting components approach. Furthermore, estimating the set of optimal tradeoffs and finding the best compromise solutions around each of the Pareto fronts may be the best method for determining the result of the multi-objective problem. The multi-objective problem should be written as follows.

$$\text{Minimize} : f_i(u), \quad i = 1, 2, 3, \ldots, N \tag{49}$$

$$\text{Subjected to: } g_j(u) = 0, \quad j = 1, 2, 3, \ldots, M \tag{50}$$

$$h_k(u) \leq 0, \quad k = 1, 2, \ldots, K \tag{51}$$

where f_i is the irrational fitness function, N indicates the total fitness function, M denotes the number of equality constraints, and K denotes the total inequality constraints. The non-dominated sorting strategy in multiobjective optimization might have two probabilities: one objective dominating the other or not. To put it another way, without losing the ability to generalize; Only if the given two requirements are met, does u_1 have the upper hand over u_2.

$$\forall i \in \{1, 2, 3 \ldots\ldots N\} : f_i(u_1) \leq f_i(u_2) \tag{52}$$

$$\exists j \in \{1, 2, 3 \ldots\ldots N\} : f_j(u_1) \leq f_j(u_2) \tag{53}$$

If any of the preceding conditions are not met, the solution u_1 is no longer in control of u_2. If u_1 outnumbers u_2, it is referred to as the non-dominated solution. The pseudocode of the MOEO is presented in the *Algorithm* [50]. The maximum function evaluations and the population size N_{pop} are control parameters of the MOEO algorithm. In addition, a random

parent population P_o is generated in search space S and every fitness function of the fitness vector F for P_o is evaluated. P_o is then subjected to non-dominated sorting and the determination of crowding distances. The MOEO method is then used to create the new population P_j, which is subsequently converged with P_o to form the combined population P_i. The best N_{pop} solutions are referred to as parent population based on non-domination sorting and calculated estimates of crowding distance and non-domination rank. This process is repeated until the maximum number of generations has been reached. It's worth noting that a similar method can be used in conjunction with the termination criteria based on the function's overall evaluations. The readers are highly recommended to read [50] for more comprehensive details.

For a non-dominated solution, the membership function score for every fitness function is first determined as follows.

$$\mu_m^k = \begin{cases} 1, & f_m^k \le f_m^{min} \\ \dfrac{f_{\mathrm{m}}^{max} - f_j^i}{f_j^{min} - f_j^{max}}, & f_{\mathrm{m}}^{min} \le f_m^k \le f_{\mathrm{m}}^{max} \\ 0, & f_m^k \ge f_m^{max} \end{cases} \tag{54}$$

where μ_m^k signifies the value of the membership function of k^{th} non-dominated solution of m^{th} objective, f_{m}^{max} and f_{m}^{min} denote the maximum and minimum objective function value of the generated non-dominated solutions, f_m^k denotes the fitness function values of k^{th} non-dominated solution of m^{th} objective. On every solution, the normalized membership function can be formed as follows.

$$\mu_k = \frac{\sum_{m=1}^{N_{obj}} \mu_m^k}{\sum_{k=1}^{N_d} \sum_{m=1}^{N_{obj}} \mu_m^k} \tag{55}$$

where N_{obj} is the number of the fitness functions and N_d represents the number of non-dominated solutions. The value with the highest μ_k value is the most compromised.

Algorithm Pseudocode of MOEO Algorithm

Step-1: Generate random population P_o in the solution set S and fitness vector F for the generatedP_o
Step-2: Categorize the P_o using non-dominated sorting process and compute the non-dominated rank and generate Pareto fronts
Step-3: Determine the crowding distance for every Pareto front generated
Step-4: Update the P_j solutions by EO algorithm
Step-5: To produce $P_i = P_o \cup P_j$, combine P_o and P_j
Step-6: For P_i, complete step-2 as per the rank and crowding distance sort P_i
Step-7: Replace P_o with P_i for first N_{pop} of P_i

V. RESULTS AND DISCUSSIONS

In this section, the validation of EO and MOEO on an enhanced IEEE-30 bus system is carried out, and the performance comparison is also made among well-established algorithms. There are two simulation scenarios considered in this section. Scenario 1 deals with the single-objective OPF problem, and Scenario 2 deals with the multi-objective OPF problem.

A. SCENARIO-1

This study uses the EO algorithm to address the probabilistic optimal power flow problem with three sustainable energy units: wind, solar, and hybrid small-hydropower. The features of the enhanced IEEE-30 bus network are listed in Table 1. Table 6 shows the entire test cases considered in this paper. The proposed strategy is developed using the MATLAB tool installed on a 3.4GHz Intel *i*5 CPU with 8 GB memory. The population size is set to 40, and each algorithm is run 10 times with 100 iterations. The EO algorithm is related to finding solutions for sustainable power generation units. The solution to the OPF problem is also verified and compared with the recently developed algorithms such as Ion Motion Optimizer (IMO) [54], Grey Wolf Optimizer (GWO) [55], and Harris Hawks Optimization (HHO) [56].

The obtained results for the case study from 1-5 are listed in Tables 7-9. Table 6 lists the decision vectors for case studies 1-2, including the best Total Fuel Cost (TFC) and the emission. The results obtained by entirely algorithms are also recorded in Table 7. Table 7 shows that the TFC value obtained by the EO is 891.651 $/hr, which is the best, followed by GWO, HHO, and IMO. Similarly, the value of emission obtained by EO is 0.092 Ton/hr, which is the best in addition to the GWO and IMO. The emission achieved by the HHO is higher than the selected algorithms.

Table 8 lists the decision vectors for case studies 3-4, including the best APL and the VD values. The results obtained by selected algorithms are also recorded in Table 8. Table 8 shows that the APL value obtained by the EO is 1.866 MW, which is the best, followed by IMO, GWO, and HHO. Similarly, the value of VD obtained by EO is 0.284 p.u., which is best followed by GWO, HHO, and IMO.

Table 9 lists the decision vectors for case study 5, including the best VSI (L-index) values. The results obtained by selected algorithms are also recorded in Table 9. From Table 9, it is noticed that the L-index value obtained by the EO is 0.133, which is similar to the selected algorithms.

Some of the traditional and well-established algorithms are called the Multi-Objective Evolutionary Algorithm with Superiority of Feasible solution constraint handling mechanism (MOEA/D-SF) and Summation-based Multi-Objective DE algorithm with Superiority of Feasible solution constraint handling mechanism (SMODE/SF) is applied for first case studies of OPF problem [34]. The consolidated results obtained by EO and other selected algorithms, including MOEA/D-SF and SMODE/SF for all case studies, are listed in Table 10. The result of TFC, including the sustainable power plants with EO, is 891.651 $/hr which is the best among the four algorithms. Also, reduced up to 1.352 $/hr in comparison with the MOEA/D-SF and 1.852 $/hr in

TABLE 6. Test cases considered in this study.

Test system	Case #	Single- and Multi-Objective Functions
IEEE 30-bus test system (Modified)	Case # 1	Minimization of the generation cost
	Case # 2	Minimization of emission
	Case # 3	Minimization of APL
	Case # 4	VD minimization
	Case # 5	Voltage Stability Index (VSI)
	Case # 6	Minimization of the TFC and PM
	Case # 7	Minimization of the TFC and APL
	Case # 8	Minimization of the TFC and VD
	Case # 9	Minimization of the TFC, PM, and APL
	Case # 10	Minimization of the TFC, PM, and VD
	Case # 11	Minimization of the TFC, PM, APL, and VD

TABLE 7. Single-objective simulation results of case-1 and case-2.

Control Parameters	Min	Max	Case-1				Case-2			
			EO	HHO	GWO	IMO	EO	HHO	GWO	IMO
$P_{G2(Thermal)}$	**20**	**80**	53.898	43.769	51.585	53.896	46.634	60.000	46.692	45.665
$P_{G8(Thermal)}$	**10**	**35**	11.052	21.638	13.195	26.000	35.000	21.072	35.000	34.936
$P_{G5(Wind)}$	**0**	**75**	51.758	52.515	50.155	42.741	74.999	75.000	75.000	74.794
$P_{G11(Solar)}$	**0**	**50**	17.610	15.556	17.480	16.198	49.657	50.000	50.000	49.888
P_{G13} (Solar+Small Hydro.)	**0**	**50**	15.223	16.915	15.988	15.801	47.005	48.512	46.611	47.097
V_1	**0.95**	**1.1**	1.099	1.100	1.100	1.100	1.099	1.100	0.955	1.100
V_2	**0.95**	**1.1**	1.089	1.094	1.095	1.100	1.090	1.100	0.971	1.100
V_5	**0.95**	**1.1**	1.070	1.079	1.070	1.100	1.026	1.100	0.953	1.100
V_8	**0.95**	**1.1**	1.071	1.086	1.081	1.100	1.098	1.100	0.986	1.100
V_{11}	**0.95**	**1.1**	1.099	1.076	1.100	1.100	1.015	1.100	0.974	1.100
V_{13}	**0.95**	**1.1**	1.099	1.096	1.089	1.100	1.065	1.100	1.070	1.100
$Q_{G1(Swing)}$	**-50**	**140**	121.787	80.974	47.802	-28.720	-11.011	140.000	138.777	139.526
$Q_{G2(Thermal)}$	**-20**	**60**	27.723	29.341	-10.679	59.999	45.647	3.865	-14.898	57.519
$Q_{G8(Thermal)}$	**-15**	**40**	25.335	39.318	9.552	22.896	4.079	16.313	-14.045	39.922
$Q_{G5(Wind)}$	**-30**	**35**	2.812	34.404	-1.561	-4.553	31.556	4.762	-0.681	34.824
$Q_{G11(Solar)}$	**-20**	**25**	-14.862	14.244	1.060	-9.800	20.060	25.000	-0.028	24.958
$Q_{G13(Solar+Small Hydro.)}$	**-20**	**25**	-19.995	24.569	-5.080	-12.953	-16.344	1.498	25.000	24.029
TFC ($/hr)			**891.651**	**893.931**	**892.060**	**896.007**	-	-	-	-
Emission (Ton/hr)			-	-	-	-	**0.092**	**0.094**	**0.092**	**0.092**

comparison with the SMODE/SF, as seen in Table 10. The boldfaces in the tables indicate the best result.

The convergence curves of entire case studies are illustrated in Figs. 6-10. As consolidated in Table 9, the EO algorithm produces the best optimal results for all case studies of single-objective OPF problems. From the convergence curves, it is observed that the EO algorithm produces the best optimal results, in addition to quick converges than the selected algorithms. For most entirely case studies of single-objective OPF, HHO produces the worst results, and the convergence speed is also poor than entire algorithms. Next to HHO, the IMO algorithm also produces worst results than the GWO and EO, apart from HHO. The results produced by the GWO are almost similar to EO for a few case studies; however, the convergence speed is slower than the EO algorithm. Therefore, from the discussions, it is discovered that the EO algorithm stood first, followed by GWO, IMO, and HHO.

Comparative analysis plots with respect to total fuel cost are shown in Fig. 11. While analyzing the simulated results of entire case studies, it is shown that the suggested EO algorithm provides the best optimal solutions.

TABLE 8. Single-objective simulation results of case-3and case-4.

Control Parameters	Min	Max	Case-3				Case-4			
			EO	HHO	GWO	IMO	EO	HHO	GWO	IMO
$P_{G2(Thermal)}$	20	80	67.051	80.000	71.222	66.066	25.983	71.719	64.032	20.000
$P_{G8(Thermal)}$	10	35	35.000	35.000	34.652	35.000	34.850	13.202	20.173	10.008
$P_{G5(Wind)}$	0	75	75.000	75.000	75.000	75.000	66.528	51.889	43.279	1.826
$P_{G11(Solar)}$	0	50	50.000	50.000	48.494	50.000	0.012	6.310	5.745	0.519
$P_{G13\ (Solar+Small\ Hydro.)}$	0	50	48.302	48.303	47.553	48.302	0.228	43.751	4.602	0.810
V_1	0.95	1.1	1.100	1.100	1.098	1.100	0.977	0.950	0.968	1.037
V_2	0.95	1.1	1.100	1.100	1.099	1.100	0.950	0.995	0.950	1.011
V_5	0.95	1.1	1.090	1.100	1.085	1.094	0.973	1.052	0.974	1.026
V_8	0.95	1.1	1.096	1.100	1.094	1.100	1.100	1.061	1.100	1.047
V_{11}	0.95	1.1	1.100	1.100	1.100	1.100	1.100	1.097	1.100	1.084
V_{13}	0.95	1.1	1.100	1.100	1.100	1.100	1.053	1.063	1.052	1.064
$Q_{G1(Swing)}$	-50	140	136.471	140.000	21.080	140.000	-22.611	-3.012	22.242	-18.873
$Q_{G2(Thermal)}$	-20	60	52.289	60.000	21.260	60.000	56.587	12.514	-2.420	35.355
$Q_{G8(Thermal)}$	-15	40	-10.424	40.000	4.157	40.000	-9.586	-12.698	4.677	23.649
$Q_{G5(Wind)}$	-30	35	34.252	35.000	-30.000	35.000	21.053	3.364	-9.509	-30.000
$Q_{G11(Solar)}$	-20	25	15.315	25.000	13.111	25.000	19.545	-1.494	8.755	-19.990
$Q_{G13(Solar+Small\ Hydro.)}$	-20	25	-18.250	25.000	2.112	25.000	-11.091	-12.410	0.698	-19.899
APL in MW			**1.866**	**1.914**	**1.899**	**1.872**	-	-	-	-
VD in p.u.			-	-	-	-	**0.284**	**0.359**	**0.290**	**0.365**

TABLE 9. Single-objective simulation results of case-5.

Control Parameters	Min	Max	Case-5			
			EO	HHO	GWO	IMO
$P_{G2(Thermal)}$	20	80	80.000	60.000	43.433	80.000
$P_{G8(Thermal)}$	10	35	35.000	35.000	35.000	35.000
$P_{G5(Wind)}$	0	75	75.000	34.764	67.390	75.000
$P_{G11(Solar)}$	0	50	34.586	9.347	36.289	31.232
$P_{G13(Solar+Small\ Hydro.)}$	0	50	0.000	22.448	3.539	5.976
V_1	0.95	1.1	1.100	1.100	1.100	1.100
V_2	0.95	1.1	1.100	1.100	1.100	1.100
V_5	0.95	1.1	1.100	1.100	1.100	1.100
V_8	0.95	1.1	1.100	1.100	1.100	1.100
V_{11}	0.95	1.1	1.100	1.100	1.100	1.100
V_{13}	0.95	1.1	1.100	1.100	1.100	1.100
$Q_{G1(Swing)}$	-50	140	104.780	54.868	-0.623	140.000
$Q_{G2(Thermal)}$	-20	60	-15.184	23.659	-5.244	60.000
$Q_{G8(Thermal)}$	-15	40	-12.450	11.625	21.957	40.000
$Q_{G5(Wind)}$	-30	35	-26.627	11.578	-9.583	35.000
$Q_{G11(Solar)}$	-20	25	-16.128	8.450	2.219	25.000
$Q_{G13(Solar+Small\ Hydro.)}$	-20	25	11.307	8.450	-18.661	25.000
L-index			**0.133**	**0.133**	**0.133**	**0.133**

B. SCENARIO-2

In this scenario, the MOEO algorithm was applied to optimize two, three, and four conflicting objectives simultaneously. The non-dominated sorting EO algorithm is used in the multiobjective OPF problems to determine the archives of different objectives simultaneously. The Pareto front for the

TABLE 10. Obtained simulation results by entirely selected algorithms.

Single Objectives Functions	EO	HHO	GWO	IMO	MOEA/D-SF	SMODE/SF
Total Fuel Cost (TFC) ($/hr)	**891.568**	893.931	892.060	896.007	893.003	893.503
Emission (Ton/hr)	**0.092**	0.094	**0.092**	**0.092**	0.1091	0.0961
VD (p.u.)	**0.284**	0.359	0.290	0.365	NA	NA
APL (MW)	**1.866**	1.911	2.069	1.889	NA	NA
VSI	**0.133**	**0.133**	**0.133**	**0.133**	NA	NA

NA-Not Available

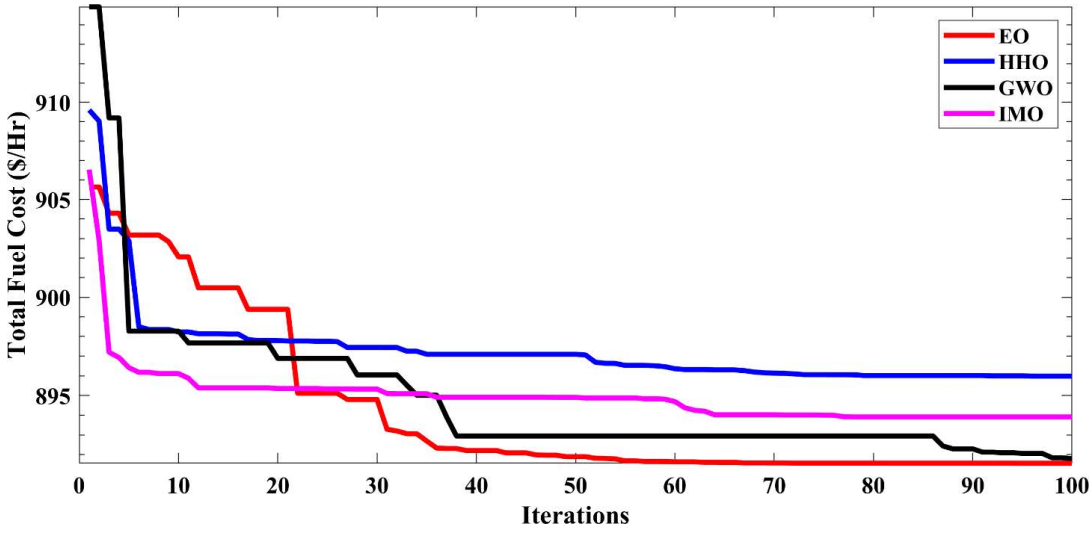

FIGURE 6. Convergence curves obtained by entirely algorithms for Case 1 (Minimization of TFC).

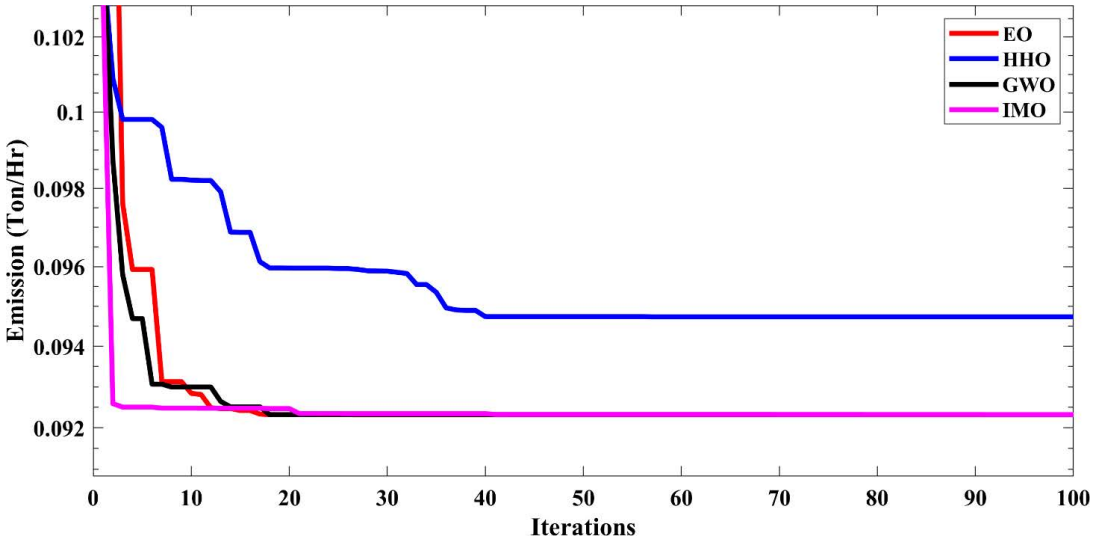

FIGURE 7. Convergence curves obtained by entirely algorithms for Case 2 (Minimization of Emission).

adapted IEEE 30-bus framework is obtained using 30 non-dominate results. Similar to the previous test scenario, scenario 2 was executed 30 times to get fair results. Cases 6 to 8 are referred to as two objectives optimization problems, whereas cases 9 and 10 are referred to as three objectives optimization problems. In case 11, entirely four objectives are optimized at the same time. The fuzzy membership function is utilized to determine the best compromising response from the Pareto archives [57], [58]. Comparing the best Pareto fronts obtained by the four established multi-objective

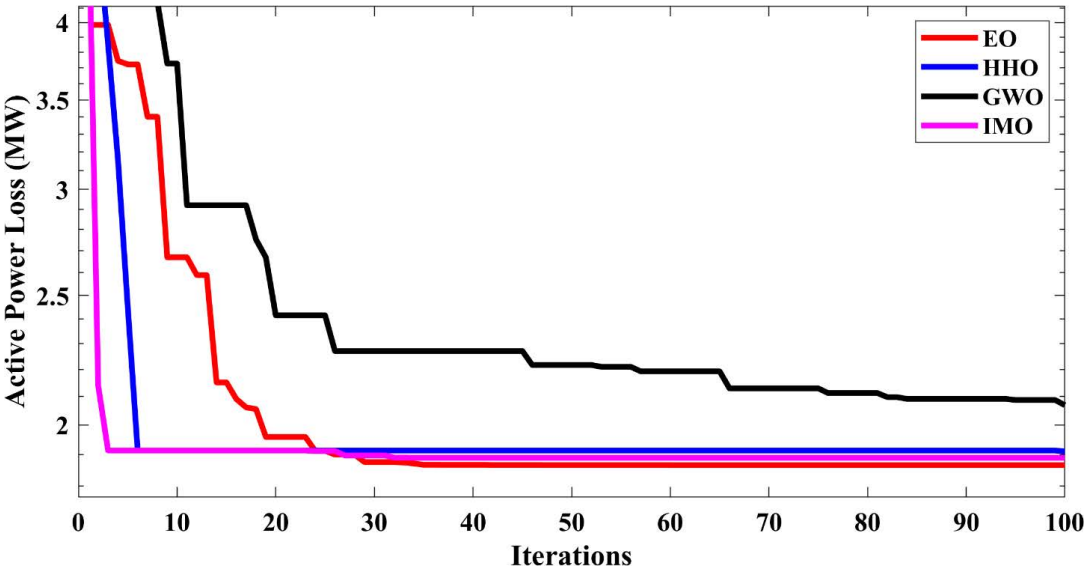

FIGURE 8. Convergence curves obtained by entirely algorithms for Case 3 (Minimization of APL).

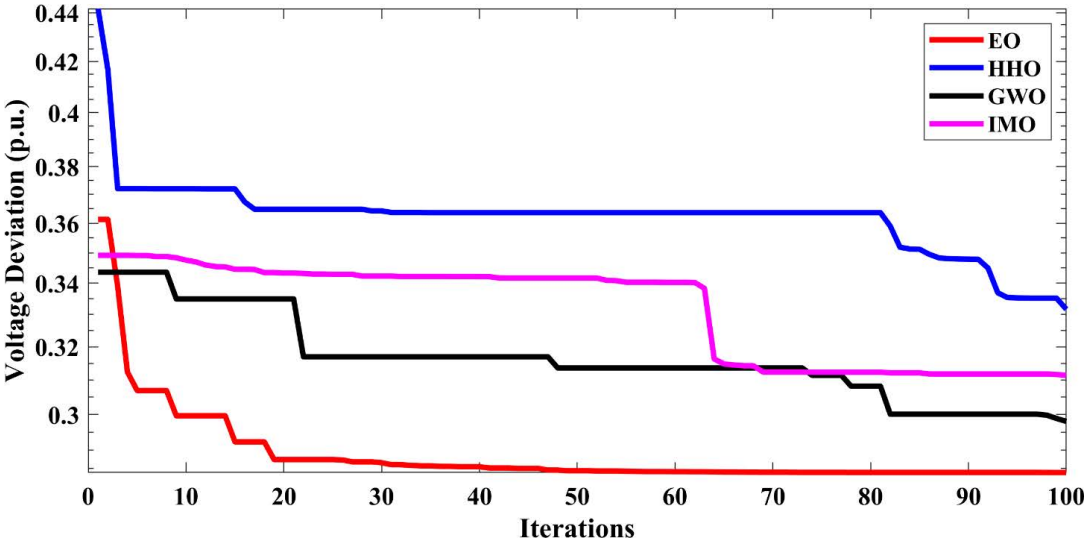

FIGURE 9. Convergence curves obtained by entirely algorithms for Case 4 (Minimization of VD).

algorithms are important. The optimal Pareto fronts generated by entirely algorithms are shown in Figs. 12(a-f). For cases 6 to 9, the best-compromised responses using the MOEO algorithm and other well-established algorithms, such as MOWOA [59], MOGWO [18], [60], and MOIMO [61], are shown in Table 11, and the best results are shown in boldface. The selected multi-objective algorithms are applied to generate the optimal Pareto fronts for case studies. The population size for entire algorithms is 30, and the maximum number of generations is 500. Other algorithmic parameters of entire algorithms are selected as per the respective base paper. The Pareto fronts obtained for Cases 6-11 are shown in Fig. 12. As seen in the Pareto fronts, MOEO has more diversity than other algorithms. In other words, the emission, TFC, APL, and VD values reached by MOEO is better than that of selected algorithms, which is true throughout trial runs.

Compliance with system constraints is a crucial part of the constraint optimization problem. In a single objective problem, dealing with constraints is challenging. The scenario is significantly more complicated for multiobjective problems, such as the OPF with stochastic renewables because the Pareto front contains numerous solutions necessary to be practicable. The Pareto front produced from every test run contains 30 non-dominated solutions, and algorithms provide feasible opportunities. However, it is not feasible to

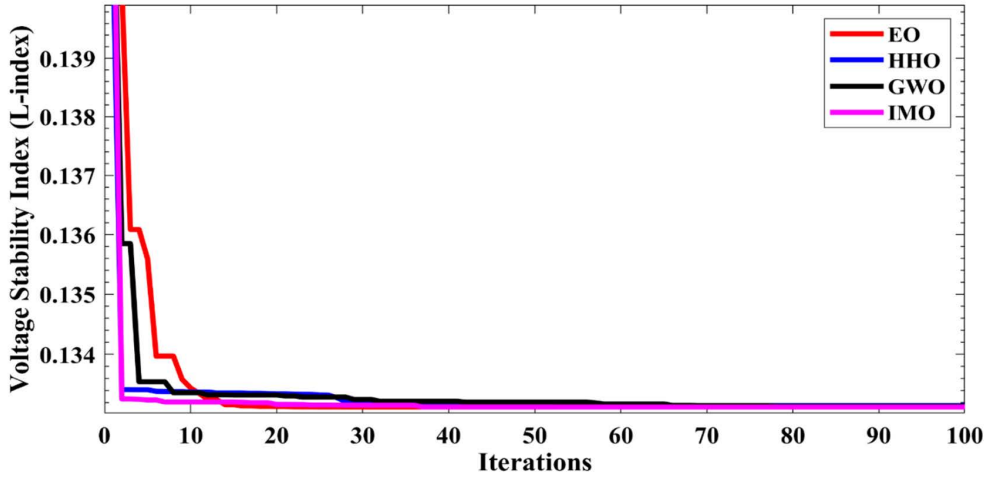

FIGURE 10. Convergence curves obtained by entirely algorithms for Case 5 (Minimization of VSI).

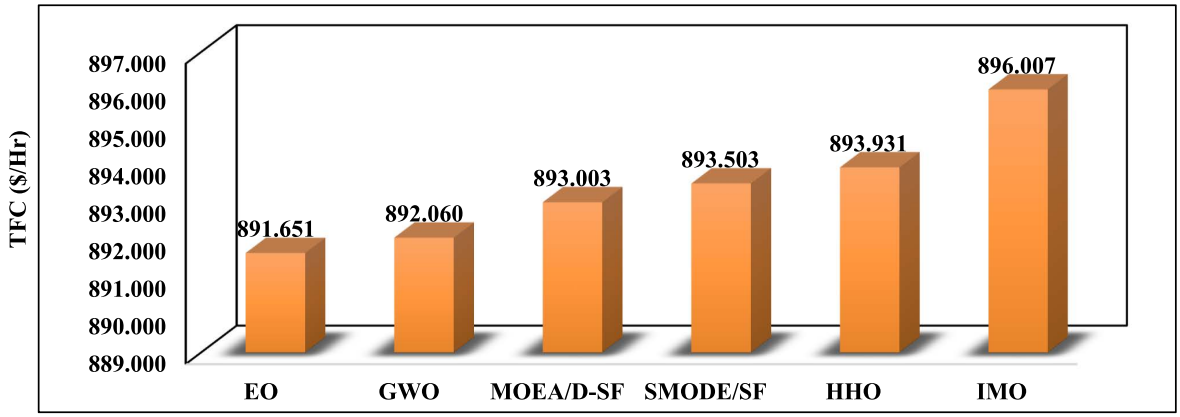

FIGURE 11. Comparison plot analysis with respect to TFC.

TABLE 11. Multi-objectives simulation results were obtained for different cases.

Multi-Objectives Functions	MOEO	MOWOA	MOGWO	MOIMO
		CASE-6		
TFC ($/hr)	**923.821**	932.679	930.661	925.810
Emission (Ton/hr)	**0.574**	0.424	0.432	0.534
		CASE-7		
TFC ($/hr)	**967.977**	967.066	975.684	967.879
APL (MW)	**3.357**	3.418	3.104	3.363
		CASE-8		
TFC ($/hr)	901.303	**899.393**	902.587	899.613
VD (p.u.)	0.349	**0.367**	0.345	0.358
		CASE-9		
TFC ($/hr)	975.734	964.521	965.231	**973.465**
Emission (Ton/hr)	0.139	0.213	0.172	**0.141**
APL (MW)	3.289	3.560	3.579	**3.282**
		CASE-10		
TFC ($/hr)	**896.392**	897.039	918.946	926.204
Emission (Ton/hr)	**2.055**	2.671	0.838	1.052
VD (p.u.)	**0.519**	0.484	0.416	0.492
		CASE-11		
TFC ($/hr)	**954.019**	943.289	966.322	951.374
Emission (Ton/hr)	**0.256**	0.909	0.311	0.297
APL (MW)	**4.543**	8.320	5.604	4.830
VD (p.u.)	**0.716**	0.518	0.595	0.423

verify all solutions at this time, and we do focus on choosing selected solutions from specific test runs and monitoring the availability of important constraints. When an EO is combined with a non-dominated sorting and crowding distance mechanism, the search process of the MOEO can be systematically guided towards optimal global solutions.

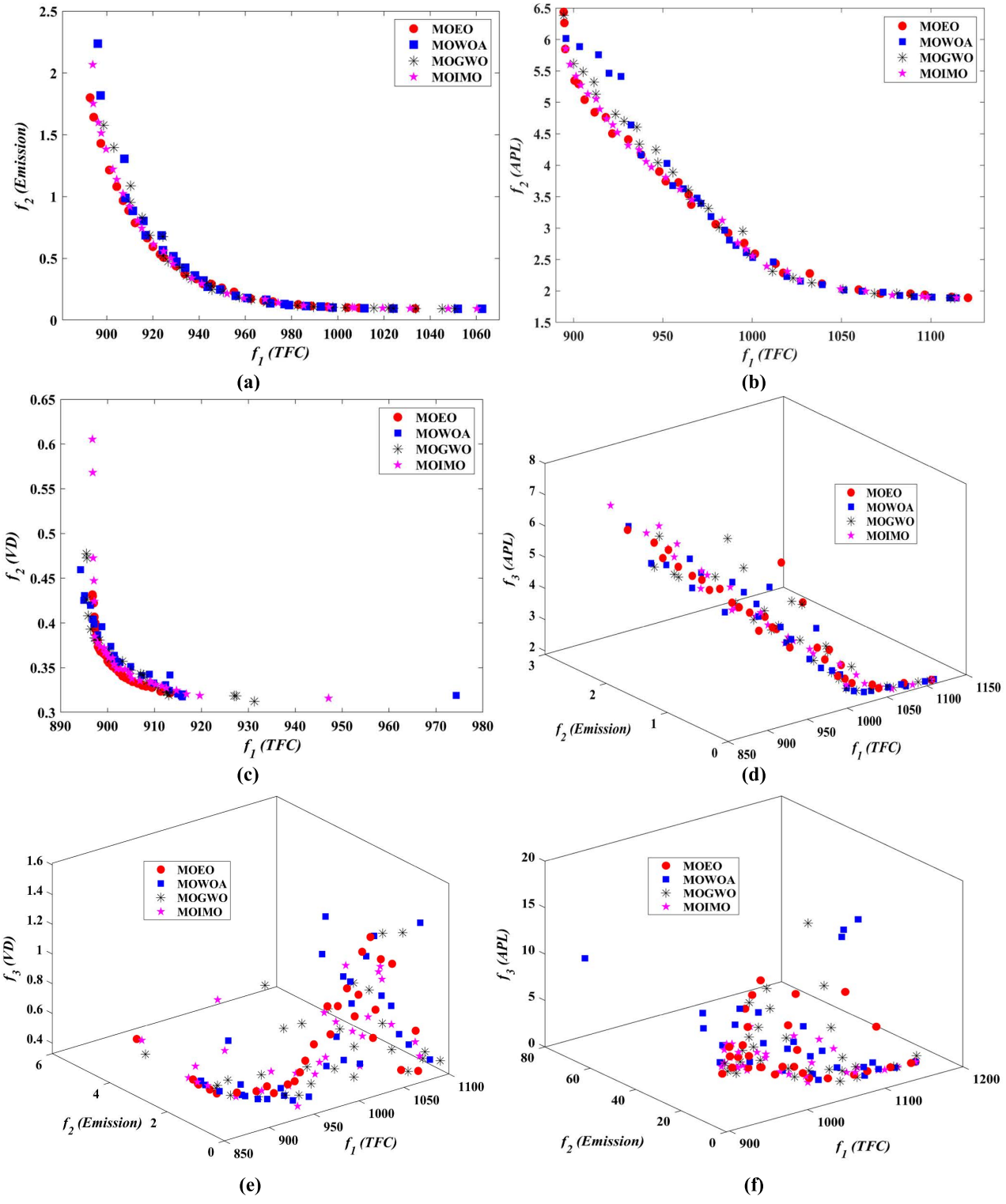

FIGURE 12. Pareto front obtained by selected algorithms, (a) Case 6, (b) Case 7, (c) Case 8, (d) Case 9, (e) Case 10, (f) Case 11.

VI. CONCLUSION

The research on OPF of hybrid power systems has become more significant in modern trends in the energy industry and environmental policy since it analyses sustainable and constantly replenished renewable resources. Therefore, this paper suggests an algorithm for locating Pareto's optimal solutions to the multiobjective OPF problem, which includes stochastic solar, wind, and hybrid small hydropower units. The renewable energy sources studied in this study have stochastic characteristics that are represented using suitable

probability density functions. The non-convex, nonlinear, and multimodal multi-objective OPF problem is solved using the MOEO algorithm and formulated using EO, non-dominated sorting, and crowding distance mechanisms. The system's constraints, notably network security constraints, have been satisfied. The obtained results are compared with several well-established algorithms. The results reveal that the suggested MOEO algorithm obtained higher quality with more practicable solutions. Without a doubt, entirely of the results suggest that the proposed algorithm has an advantage in achieving optimal solutions to single- and multi-objective OPF problems.

In future studies, the MOEO algorithm may also be applied to other engineering problems, including cyber security, demand forecasting, motor design, optimal reactive power dispatch, compensator location, transformer design, load scheduling, distribution planning, and many more.

REFERENCES

[1] M. Ebeed and S. H. E. A. Aleem, "Overview of uncertainties in modern power systems: Uncertainty models and methods," *Uncertainties Modern Power Syst.*, vol. 1, no. 1, pp. 1–34, 2021, doi: 10.1016/B978-0-12-820491-7.00001-3.

[2] A. R. Jordehi, "Scheduling heat and power microgrids with storage systems, photovoltaic, wind, geothermal power units and solar heaters," *J. Energy Storage*, vol. 41, Sep. 2021, Art. no. 102996, doi: 10.1016/J.EST.2021.102996.

[3] J. A. Laghari, H. Mokhlis, A. H. A. Bakar, and H. Mohamad, "Application of computational intelligence techniques for load shedding in power systems: A review," *Energy Convers. Manage.*, vol. 75, pp. 130–140, Nov. 2013, doi: 10.1016/j.enconman.2013.06.010.

[4] A. X. R. Irudayaraj, N. I. A. Wahab, M. Premkumar, M. A. M. Radzi, N. B. Sulaiman, V. Veerasamy, R. A. Farade, and M. Z. Islam, "Renewable sources-based automatic load frequency control of interconnected systems using chaotic atom search optimization," *Appl. Soft Comput.*, vol. 119, Apr. 2022, Art. no. 108574, doi: 10.1016/J.ASOC.2022.108574.

[5] D. Menaga, M. Premkumar, R. Sowmya, and S. Narasimman, "Design of nonlinear uncertainty controller for grid-tied solar photovoltaic system using sliding mode control," *Energy Eng.*, vol. 117, no. 6, pp. 481–495, 2020, doi: 10.32604/EE.2020.013282.

[6] H. Abdi, S. D. Beigvand, and M. La Scala, "A review of optimal power flow studies applied to smart grids and microgrids," *Renew. Sustain. Energy Rev.*, vol. 71, pp. 742–766, May 2017, doi: 10.1016/J.RSER.2016.12.102.

[7] J. Luo, L. Shi, and Y. Ni, "A solution of optimal power flow incorporating wind generation and power grid uncertainties," *IEEE Access*, vol. 6, pp. 19681–19690, 2018, doi: 10.1109/ACCESS.2018.2823982.

[8] R. Jamal, B. Men, and N. H. Khan, "A novel nature inspired meta-heuristic optimization approach of GWO optimizer for optimal reactive power dispatch problems," *IEEE Access*, vol. 8, pp. 202596–202610, 2020, doi: 10.1109/ACCESS.2020.3031640.

[9] R. Ma, X. Li, W. Gao, P. Lu, and T. Wang, "Random-fuzzy chance-constrained programming optimal power flow of wind integrated power considering voltage stability," *IEEE Access*, vol. 8, pp. 217957–217966, 2020, doi: 10.1109/ACCESS.2020.3040382.

[10] J. L. Carpentier, "Optimal power flows: Uses, methods and developments," *IFAC Proc. Volumes*, vol. 18, no. 7, pp. 11–21, Jul. 1985, doi: 10.1016/S1474-6670(17)60410-5.

[11] W. D. Rosehart, C. A. Cañizares, and V. H. Quintana, "Multiobjective optimal power flows to evaluate voltage security costs in power networks," *IEEE Trans. Power Syst.*, vol. 18, no. 2, pp. 578–587, May 2003, doi: 10.1109/TPWRS.2003.810895.

[12] D. Sun, B. Ashley, B. Brewer, A. Hughes, and W. Tinney, "Optimal power flow by Newton approach," *IEEE Trans. Power App. Syst.*, vols. PAS–103, no. 10, pp. 2864–2880, Oct. 1984, doi: 10.1109/TPAS.1984.318284.

[13] P. P. Biswas, P. N. Suganthan, and G. A. J. Amaratunga, "Optimal power flow solutions incorporating stochastic wind and solar power," *Energy Convers. Manage.*, vol. 148, pp. 1194–1207, Sep. 2017, doi: 10.1016/j.enconman.2017.06.071.

[14] P. P. Biswas, P. N. Suganthan, R. Mallipeddi, and G. A. J. Amaratunga, "Optimal power flow solutions using differential evolution algorithm integrated with effective constraint handling techniques," *Eng. Appl. Artif. Intell.*, vol. 68, pp. 81–100, Feb. 2018, doi: 10.1016/j.engappai.2017.10.019.

[15] Y. Zhu, B. Qiao, Y. Dong, B. Qu, and D. Wu, "Multiobjective dynamic economic emission dispatch using evolutionary algorithm based on decomposition," *IEEJ Trans. Electr. Electron. Eng.*, vol. 14, no. 9, pp. 1323–1333, Sep. 2019, doi: 10.1002/tee.22933.

[16] Y. Zhu, J. Wang, and B. Qu, "Multi-objective economic emission dispatch considering wind power using evolutionary algorithm based on decomposition," *Int. J. Electr. Power Energy Syst.*, vol. 63, pp. 434–445, Dec. 2014, doi: 10.1016/j.ijepes.2014.06.027.

[17] H. Ma, Z. Yang, P. You, and M. Fei, "Multi-objective biogeography-based optimization for dynamic economic emission load dispatch considering plug-in electric vehicles charging," *Energy*, vol. 135, pp. 101–111, Sep. 2017, doi: 10.1016/J.ENERGY.2017.06.102.

[18] P. Jangir and N. Jangir, "A new non-dominated sorting grey wolf optimizer (NS-GWO) algorithm: Development and application to solve engineering designs and economic constrained emission dispatch problem with integration of wind power," *Eng. Appl. Artif. Intell.*, vol. 72, pp. 449–467, Jun. 2018, doi: 10.1016/j.engappai.2018.04.018.

[19] B. Dey, B. Bhattacharyya, S. Raj, and R. Babu, "Economic emission dispatch on unit commitment-based microgrid system considering wind and load uncertainty using hybrid MGWOSCACSA," *J. Electr. Syst. Inf. Technol.*, vol. 7, no. 1, pp. 1–26, Oct. 2020, doi: 10.1186/S43067-020-00023-6.

[20] J. B. Hmida, T. Chambers, and J. Lee, "Solving constrained optimal power flow with renewables using hybrid modified imperialist competitive algorithm and sequential quadratic programming," *Electric Power Syst. Res.*, vol. 177, Dec. 2019, Art. no. 105989, doi: 10.1016/J.EPSR.2019.105989.

[21] S. Y. Abujarad, M. W. Mustafa, and J. J. Jamian, "Recent approaches of unit commitment in the presence of intermittent renewable energy resources: A review," *Renew. Sustain. Energy Rev.*, vol. 70, pp. 215–223, Apr. 2017, doi: 10.1016/J.RSER.2016.11.246.

[22] K. Sureshkumar and V. Ponnusamy, "Hybrid renewable energy systems for power flow management in smart grid using an efficient hybrid technique," *Trans. Inst. Meas. Control*, vol. 42, no. 11, pp. 2068–2087, Jul. 2020, doi: 10.1177/0142331220904818.

[23] L. L. Lai, J. T. Ma, R. Yokoyama, and M. Zhao, "Improved genetic algorithms for optimal power flow under both normal and contingent operation states," *Int. J. Electr. Power Energy Syst.*, vol. 19, no. 5, pp. 287–292, Jun. 1997, doi: 10.1016/S0142-0615(96)00051-8.

[24] M. A. Abido, "Optimal power flow using particle swarm optimization," *Int. J. Elect. Power Energy Syst.*, vol. 24, no. 7, pp. 563–571, Oct. 2002, doi: 10.1016/S0142-0615(01)00067-9.

[25] B. E. Turkay and R. I. Cabadag, "Optimal power flow solution using particle swarm optimization algorithm," in *Proc. EuroCon*, Jul. 2013, pp. 1418–1424, doi: 10.1109/EUROCON.2013.6625164.

[26] U. Khaled, A. M. Eltamaly, and A. Beroual, "Optimal power flow using particle swarm optimization of renewable hybrid distributed generation," *Energies*, vol. 10, no. 7, p. 1013, Jul. 2017, doi: 10.3390/EN10071013.

[27] S. R. Salkuti, "Optimal power flow using multi-objective glowworm swarm optimization algorithm in a wind energy integrated power system," *Int. J. Green Energy*, vol. 16, no. 15, pp. 1547–1561, 2019, doi: 10.1080/15435075.2019.1677234.

[28] H. R. E. H. Bouchekara, A. E. Chaib, M. A. Abido, and R. A. El-Sehiemy, "Optimal power flow using an improved colliding bodies optimization algorithm," *Appl. Soft Comput.*, vol. 42, pp. 119–131, May 2016, doi: 10.1016/J.ASOC.2016.01.041.

[29] A. A. El Ela, M. Abido, and S. R. Spea, "Optimal power flow using differential evolution algorithm," *Electr. Eng.*, vol. 80, no. 7, pp. 878–885, Jul. 2010, doi: 10.1016/J.EPSR.2009.12.018.

[30] J. C. Bansal, S. S. Jadon, R. Tiwari, D. Kiran, and B. K. Panigrahi, "Optimal power flow using artificial bee colony algorithm with global and local neighborhoods," *Int. J. Syst. Assurance Eng. Manage.*, vol. 8, no. 4, pp. 2158–2169, Dec. 2017, doi: 10.1007/S13198-014-0321-7.

[31] A.-A. A. Mohamed, Y. S. Mohamed, A. A. M. El-Gaafary, and A. M. Hemeida, "Optimal power flow using moth swarm algorithm," *Electr. Power Syst. Res.*, vol. 142, pp. 190–206, Jan. 2017, doi: 10.1016/J.EPSR.2016.09.025.

[32] R. Chi, Z. Li, X. Chi, Z. Qu, and H.-B. Tu, "Reactive power optimization of power system based on improved differential evolution algorithm," *Math. Problems Eng.*, vol. 2021, pp. 1–19, Feb. 2021, doi: 10.1155/2021/6690924.

[33] P. P. Biswas, P. N. Suganthan, R. Mallipeddi, and G. A. J. Amaratunga, "Multi-objective optimal power flow solutions using a constraint handling technique of evolutionary algorithms," *Soft Comput.*, vol. 24, no. 4, pp. 2999–3023, Feb. 2020, doi: 10.1007/s00500-019-04077-1.

[34] P. P. Biswas, P. N. Suganthan, B. Y. Qu, and G. A. J. Amaratunga, "Multiobjective economic-environmental power dispatch with stochastic wind-solar-small hydro power," *Energy*, vol. 150, pp. 1039–1057, May 2018, doi: 10.1016/j.energy.2018.03.002.

[35] T. T. Nguyen, "A high performance social spider optimization algorithm for optimal power flow solution with single objective optimization," *Energy*, vol. 171, pp. 218–240, Mar. 2019, doi: 10.1016/J.ENERGY.2019.01.021.

[36] W. Warid, H. Hizam, N. Mariun, and N. I. Abdul-Wahab, "Optimal power flow using the Jaya algorithm," *Energies*, vol. 9, no. 9, p. 678, Aug. 2016, doi: 10.3390/EN9090678.

[37] R. Roy and H. T. Jadhov, "Optimal power flow solution of power system incorporating stochastic wind power using Gbest guided artificial bee colony algorithm," *Int. J. Elect. Power Energy Syst.*, vol. 64, pp. 562–578, Jan. 2015, doi: 10.1016/J.IJEPES.2014.07.010.

[38] A. Panda and M. Tripathy, "Optimal power flow solution of wind integrated power system using modified bacteria foraging algorithm," *Int. J. Elect. Power Energy Syst.*, vol. 54, pp. 306–314, Jan. 2014, doi: 10.1016/J.IJEPES.2013.07.018.

[39] A. Panda and M. Tripathy, "Security constrained optimal power flow solution of wind-thermal generation system using modified bacteria foraging algorithm," *Energy*, vol. 93, pp. 816–827, Dec. 2015, doi: 10.1016/J.ENERGY.2015.09.083.

[40] L. Shi, C. Wang, L. Yao, Y. Ni, and M. Bazargan, "Optimal power flow solution incorporating wind power," *IEEE Syst. J.*, vol. 6, no. 2, pp. 233–241, Jun. 2012, doi: 10.1109/JSYST.2011.2162896.

[41] R. A. Jabr and B. C. Pal, "Intermittent wind generation in optimal power flow dispatching," *IET Gener., Transmiss. Distrib.*, vol. 3, no. 1, pp. 66–74, Jan. 2009, doi: 10.1049/IET-GTD:20080273.

[42] S. Mishra, Y. Mishra, and S. Vignesh, "Security constrained economic dispatch considering wind energy conversion systems," in *Proc. IEEE Power Energy Soc. Gen. Meeting*, Jul. 2011, doi: 10.1109/PES.2011.6039544.

[43] W. Zhou, Y. Peng, and H. Sun, "Optimal wind-thermal coordination dispatch based on risk reserve constraints," *Eur. Trans. Electr. Power*, vol. 21, no. 1, pp. 740–756, Jan. 2011, doi: 10.1002/ETEP.474.

[44] H. M. Dubey, M. Pandit, and B. K. Panigrahi, "Hybrid flower pollination algorithm with time-varying fuzzy selection mechanism for wind integrated multi-objective dynamic economic dispatch," *Renew. Energy*, vol. 83, pp. 188–202, Nov. 2015, doi: 10.1016/J.RENENE.2015.04.034.

[45] H. Tazvinga, B. Zhu, and X. Xia, "Optimal power flow management for distributed energy resources with batteries," *Energy Convers. Manage.*, vol. 102, pp. 104–110, Sep. 2015, doi: 10.1016/J.ENCONMAN.2015.01.015.

[46] K. Kusakana, "Optimal scheduling for distributed hybrid system with pumped hydro storage," *Energy Convers. Manage.*, vol. 111, pp. 253–260, Mar. 2016, doi: 10.1016/J.ENCONMAN.2015.12.081.

[47] S. Surender Reddy, P. R. Bijwe, and A. R. Abhyankar, "Real-time economic dispatch considering renewable power generation variability and uncertainty over scheduling period," *IEEE Syst. J.*, vol. 9, no. 4, pp. 1440–1451, Dec. 2015, doi: 10.1109/JSYST.2014.2325967.

[48] S. S. Reddy, "Optimal scheduling of thermal-wind-solar power system with storage," *Renew. Energy*, vol. 101, pp. 1357–1368, Feb. 2017, doi: 10.1016/J.RENENE.2016.10.022.

[49] A. Faramarzi, M. Heidarinejad, B. Stephens, and S. Mirjalili, "Equilibrium optimizer: A novel optimization algorithm," *Knowl.-Based Syst.*, vol. 191, Mar. 2020, Art. no. 105190, doi: 10.1016/j.knosys.2019.105190.

[50] M. Premkumar, P. Jangir, R. Sowmya, H. H. Alhelou, S. Mirjalili, and B. S. Kumar, "Multi-objective equilibrium optimizer: Framework and development for solving multi-objective optimization problems," *J. Comput. Design Eng.*, vol. 9, no. 1, pp. 24–50, Dec. 2021, doi: 10.1093/JCDE/QWAB065.

[51] M. Premkumar, P. Jangir, and R. Sowmya, "MOGBO: A new multi-objective gradient-based optimizer for real-world structural optimization problems," *Knowl.-Based Syst.*, vol. 218, Apr. 2021, Art. no. 106856, doi: 10.1016/j.knosys.2021.106856.

[52] P. Jangir, H. Buch, S. Mirjalili, and P. Manoharan, "MOMPA: Multi-objective marine predator algorithm for solving multi-objective optimization problems," *Evol. Intell.*, pp. 1–27, Aug. 2021, doi: 10.1007/S12065-021-00649-Z.

[53] S. Kumar, P. Jangir, G. G. Tejani, and M. Premkumar, "MOTEO: A novel physics-based multiobjective thermal exchange optimization algorithm to design truss structures," *Knowl.-Based Syst.*, vol. 242, Apr. 2022, Art. no. 108422, doi: 10.1016/J.KNOSYS.2022.108422.

[54] B. Javidy, A. Hatamlou, and S. Mirjalili, "Ions motion algorithm for solving optimization problems," *Appl. Soft Comput.*, vol. 32, pp. 72–79, Jul. 2015, doi: 10.1016/j.asoc.2015.03.035.

[55] S. Mirjalili, S. M. Mirjalili, and A. Lewis, "Grey wolf optimizer," *Adv. Eng. Softw.*, vol. 69, pp. 46–61, Mar. 2014, doi: 10.1016/j.advengsoft.2013.12.007.

[56] A. A. Heidari, S. Mirjalili, H. Faris, I. Aljarah, M. Mafarja, and H. Chen, "Harris hawks optimization: Algorithm and applications," *Future Gener. Comput. Syst.*, vol. 97, pp. 849–872, Aug. 2019, doi: 10.1016/j.future.2019.02.028.

[57] M. Premkumar, P. Jangir, B. S. Kumar, R. Sowmya, H. H. Alhelou, L. Abualigah, A. R. Yildiz, and S. Mirjalili, "A new arithmetic optimization algorithm for solving real-world multiobjective CEC-2021 constrained optimization problems: Diversity analysis and validations," *IEEE Access*, vol. 9, pp. 84263–84295, 2021, doi: 10.1109/ACCESS.2021.3085529.

[58] M. Premkumar, P. Jangir, R. Sowmya, H. H. Alhelou, A. A. Heidari, and H. Chen, "MOSMA: Multi-objective slime mould algorithm based on elitist non-dominated sorting," *IEEE Access*, vol. 9, pp. 3229–3248, 2021, doi: 10.1109/ACCESS.2020.3047936.

[59] P. Jangir and N. Jangir, "Non-dominated sorting whale optimization algorithm," *Global J. Researches Eng.*, vol. 17, no. 4, pp. 15–42, 2017.

[60] M. Premkumar, P. Jangir, B. Santhosh Kumar, M. A. Alqudah, and K. S. Nisar, "Multi-objective grey wolf optimization algorithm for solving real-world BLDC motor design problem," *Comput., Mater. Continua*, vol. 70, no. 2, pp. 2435–2452, 2022, doi: 10.32604/CMC.2022.016488.

[61] H. Buch and I. Trivedi, "Ions motion optimization algorithm for multi-objective optimization problems," *Decis. Sci. Lett.*, vol. 10, pp. 93–110, 2021, doi: 10.5267/J.DSL.2020.12.001.

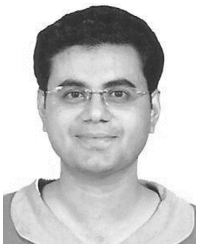

SUNDARAM B. PANDYA was born in Gujarat, India. He received the B.E. degree in electrical engineering from The M. S. University of Baroda, Vadodara, the M.E. degree in electrical engineering from Gujarat Technological University, Ahmedabad, and the Ph.D. degree from the Sardar Vallabhbhai National Institute of Technology (S. V. N. I. T, SURAT), Surat, India. He is currently working as a Lecturer with the Shri K. J. Polytechnic, Bharuch, India, under the Gujarat Educational Services. He has more than ten years of experience in teaching. He has published more than 14 technical articles in various national/international peer-reviewed journals, such as IEEE and Taylor & Francis. His research interests include application of artificial intelligence techniques in power systems, i.e power system engineering optimization, single and multi-objective optimization, swarm intelligence, evolutionary algorithms, and artificial neural networks. He is working on the applications of renewable energy resources in power system analysis and control.

SOWMYA RAVICHANDRAN received the B.E. degree in electrical and electronics engineering from the Saranathan College of Engineering, Tiruchirappalli, India, in 2013, and the M.Tech. degree in energy engineering from the National Institute of Technology, Tiruchirappalli, in 2015, where she is currently pursuing the Ph.D. degree. She worked as an Assistant Professor with the Department of Electrical and Electronics Engineering, KPR Institute of Engineering and Technology, Coimbatore, India, for the academic year 2015–2016, and worked as an Assistant Professor with the Department of Power Engineering, GMR Institute of Engineering and Technology, Rajam, India, during the academic year 2016–2017. Her research interests include control systems, electric vehicle, and renewable energy.

PREMKUMAR MANOHARAN (Member, IEEE) was born in Coimbatore, India. He received the B.E. degree in electrical and electronics engineering from the Sri Ramakrishna Institute of Technology, Coimbatore, in 2004, the M.E. degree in applied electronics from the Anna University of Technology, Coimbatore, in 2010, and the Ph.D. degree from Anna University, Chennai, India, in 2019. He is currently working as an Associate Professor with the Dayananda Sagar College of Engineering, Bengaluru, India. He has over 14 years of teaching experience. He has published more than 100 technical articles in various national/international peer-reviewed journals, such as IEEE, Elsevier, and Springer, with over 1200 citations and an H-index of 18. He has published/granted four patents by IPR, India, and IPR, Australia. His current research interests include optimization algorithms, including single-, multi-, and many-objectives for different real-world engineering design problems, power converters/inverters, PV parameter extraction, PV MPPT, PV array faults, smart grid and microgrids, BMS for electric vehicles, and non-isolated/isolated dc-dc converters for renewable energy systems and EVs. He is a member of various professional bodies, such as IEEE, ISTE, and IAENG. He is also serving as an editor/a reviewer for leading journals of different publishers, such as IEEE, IET, Wiley, Taylor & Francis, Springer, and MDPI.

PRADEEP JANGIR is currently the Co-Director of the Zero Laboratory Optimization, Gujarat, and a Power Engineer at RVPN Jaipur, Rajasthan, India. He is internationally recognized for his advances in swarm intelligence and optimization. He has published over 90 publications with over 2100 citations and an H-index of 24. His research interests include many-objective, robust optimization, power system engineering optimization, multi-objective optimization, swarm intelligence, evolutionary algorithms, and artificial neural networks. He is working on the application of multi-objective, many-objective, and robust meta-heuristic optimization techniques as well.

HASSAN HAES ALHELOU (Senior Member, IEEE) received the B.Sc. degree (Hons.) from Tishreen University, Syria, in 2011, and the M.Sc. and Ph.D. degrees (Hons.) from the Isfahan University of Technology, Iran. He is currently with the Department of Electrical and Computer Systems Engineering, Monash University, Clayton, VIC, Australia. He is also a Professor and a Faculty Member at Tishreen University and a Consultant with Sultan Qaboos University (SQU), Oman. Previously, he was with the School of Electrical and Electronic Engineering, University College Dublin (UCD), Dublin, Ireland, from 2020 to 2021, and the Isfahan University of Technology (IUT), Iran. He has published more than 200 research papers in high-quality peer-reviewed journals and international conferences. He has participated in more than 15 international industrial projects over the globe. His research papers received more than 3800 citations with H-index of 33 and i-index of 79. He has authored/edited 15 books published in reputed publishers, such as Springer, IET, Wiley, Elsevier, and Taylor & Francis. His major research interests include renewable energy systems, power systems, power system security, power system dynamics, power system cybersecurity, power system operation, control, dynamic state estimation, frequency control, smart grids, micro-grids, demand response, and load shedding. He was a recipient of the Outstanding Reviewer Award from many journals, such as *Energy Conversion and Management* (ECM), *ISA Transactions*, and *Applied Energy*, and the Best Young Researcher Award in the Arab Student Forum Creative among 61 researchers from 16 countries from Alexandria University, Egypt, in 2011. He also received the Excellent Paper Award 2021/2022 from the IEEE CSEE Journal of Power and Energy Systems (SCI IF: 3.938; Q1). He was included in the 2018 and 2019 Publons and Web of Science (WoS) list of the top 1% best reviewer and researchers in the field of engineering and cross-fields over the world. He serves as an Editor in a number of prestigious journals, such as IEEE Systems Journal, *Computers and Electrical Engineering* (CAEE) (Elsevier), *IET Journal of Engineering*, and *Smart Cities*. He has also performed more than 800 reviews for high prestigious journals, including IEEE Transactions on Power Systems, IEEE Transactions on Smart Grid, IEEE Transactions on Industrial Informatics, IEEE Transactions on Industrial Electronics, *Energy Conversion and Management*, *Applied Energy*, and *International Journal of Electrical Power and Energy Systems*.